# Atomic Layer Depositiont

## For Synthesis of

# Ceramic

## Tight UF Membrane

Jingwen Li

TU Delft Delft University of Technology

# Atomic Layer Deposition for Synthesis of Ceramic Tight UF Membrane

MSc. Civil Engineering and Geoscience
Thesis

**Jingwen Li**

Supervisors:

| | |
|---|---|
| Prof. dr. ir. Luuk Rietveld, | Technische Universiteit Delft |
| Dr. ir. Bas Heijman, | Technische Universiteit Delft |
| Dr. Ir. Ran Shang, | Technische Universiteit Delft |

Co-reader:

| | |
|---|---|
| ir. Frank Dirne, | Kavli Nanolab Delft |

# Acknowledgements

If the three-year study is a long journey, I feel grateful for many people who accompanied me through this journey. Without any single of you, I would not make it, let alone complete this master thesis.

Firstly, I would like to express my thankfulness to Luuk Rietveld and Bas heijman for giving the guidance, inspiring me with great ideas. I have learned much from their critical but constructive thinking, and will always be grateful for that. I am particularly grateful for Ran Shang's valuable and constructive suggestions, and patience during the planning and development of this thesis work. He spent countless time on discussing the ideas with me, and even more time on reviewing the drafts. Under his guidance I successfully overcame many difficulties and learned a lot. I would also like to offer my thanks to Frank Dirne and Marc for the assistance and guidance during my experiments in Kavli Lab and constructive feedback on improving the report.

My earnest thanks to many fellows and technicians of the laboratory of the department, Franca, Irene, Mohammed for their help in introducing me the experiment setup and offering me the resources in running the program. Most of the results described in this thesis would not have been obtained without their support.

It's my fortune to gratefully thank all my friends from Delft Fellowship, who were always beside me during the happy and hard moments to push me and motivate me. It was such a blessing to meet all of you.

Finally, I acknowledge the people who mean a lot to me, my Dad and Mom, for showing faith in me and giving me liberty to choose what I desired. 亲爱的爸爸，妈妈，谢谢你们一直以来无私的爱与关怀。不管遇到怎样的困难，你们总是安慰我鼓励我，给予我满满的的信任。谢谢你们一直都在，永远爱你们。要特别得谢谢我可爱的弟弟，灏文。谢谢你对我的理解和支持，谢谢你陪伴着爸爸妈妈，你勇敢得承担了许多责任，也教会了我很多。

I owe thanks to a very special person, my fiancé, Roger for his continued and unfailing love. The life during this period could be unimaginably harder if it was not your support and understanding that accompanied me through this long. You were always beside me even at times I thought that it was impossible to continue. I will always value his contribution and greatly cherish his belief in me.

I thank the Almighty for giving me the strength, patience and passion to work through all these days so that today I can stand here with my heart in joy and peace.

*Jingwen Li*
*Delft, March 2018*

# Abstract

Ceramic membranes are gaining more and more attention due to their inherent advantages compared with polymeric membranes. Their high thermal, mechanical and chemical stability make them more applicable in treating e.g. corrosive and hot wastewater. With their small pore sizes, the ceramic tight ultrafiltration (tight UF) membranes show a greater selectivity than ceramic UF or microfiltration (MF) membranes. However, low permeability and unstable membrane quality were observed using most commercially available ceramic tight UF membranes.

Atomic layer deposition (ALD), have come up as an important technique for depositing thin films, and have turned out to be a good potential alternative to produce tight UF ceramic membranes from ceramic UF or MF membranes, due to its capability of controlled deposition of a one single atom layer film.

In this study, we explored the potential of ALD in the fabrication of tight UF ceramic membranes from normal sol-gel made UF ceramic membranes with various initial pore sizes. Since the resistance against flux within a porous membrane is mainly from the separation layer, we primarily focused on the coating depth of the coated membranes by the ALD technology. In addition a relation was found between the coating depth and the performance of the coated membranes.

The results of the experiments demonstrate that ALD method could successfully be used in the fabrication of tight UF ceramic membranes and, to some extent, cure the defects in the original membranes. By applying different ALD settings, different coating depths in the membrane filtration layer were achieved, which influenced the water permeability and solute rejection. Further, membranes with larger pore sizes tended to have a deeper effective coating depth since the precursors could diffuse more easily through the larger pores. The Carmen Kozeny model, used to determine the permeability and porosity for each studied membrane, showed results in the same order of magnitude with most of the measurement data, being thus able to predict permeability as a function of porosity and layer thickness.

# Nomenclature

**List of acronyms**

| | |
|---|---|
| **MF** | Microfiltration |
| **UF** | Ultrafiltration |
| **NF** | Nanofiltration |
| **RO** | Reverse Osmosis |
| **ALD** | Atomic Layer Deposition |
| **PEALD** | Plasma-enhanced Atomic Layer Deposition |
| **MW** | Molecular Weight |
| **MWCO** | Molecular Weight Cut-off |
| **TMP** | Transmembrane Pressure |
| **PEGs** | Polyethylene Glycols |
| **SEC** | Size Exclusive Chromatography |
| **HPLC** | High-Performance Liquid Chromatography |
| **CVD** | Chemical Vapour Deposition |
| **SEM** | Scanning Electron Microscope |
| **SE** | Secondary Electrons |
| **EDX** | Energy Dispersive X-ray |
| **TMA** | Trimethylaluminium |
| **TTIP** | Titanium Isopropoxide |
| **GPC** | Growth Rate Per Cycle |

**List of symbols**

| | |
|---|---|
| cm | centimeter |
| km | kilometer |
| m | meter |
| Da | Dalton |
| Pa | pascal |
| $\mu$m | micro meter |
| nm | nanometer |
| | |
| $L_p$ | pure water permeability, $L/(m^2\ h$ bar) |
| $J$ | flux, $m^3/(m^2 \cdot s)$ |
| $T$ | temperature, °C |
| $\Delta P$ | measured TMP, Pa |
| $R$ | retention rate of PEGs, % |
| | |
| $\eta$ | viscosity |
| $\rho$ | density of the fluid, $kg/m^3$ |
| $\varepsilon$ | membrane porosity, - |
| $\tau$ | tortuosity factor, - |
| $\mu$ | viscosity of the fluid, pa$\cdot s$ |

# Contents

# 1

# Introduction

## 1.1. Background on Ceramic Membranes in Water Treatment

### 1.1.1. Development of Ceramic Membranes

Membranes play an important role in separation industry, nevertheless, they were not considered technically important until mid-1970. Since the middle of twentieth century, synthetic membranes have got more attention and have been successfully used in many industrial applications (Basile and Nunes, 2011; Wenten, 2002; Strathmann, 2001). Membrane separation is a physical process where some compounds can pass through the pores inside the membranes while others are retained. The selectivity of certain material thus depends on the combination of the nature of feed compounds, the properties of the membrane and the interaction between them.

Both polymeric and inorganic materials are used to fabricate membranes, which might have a dense or porous layer depending on their use and applications. Most commercially utilized synthetic membranes, used in water treatment, are made of polymeric materials (Gitis and Rothenberg, 2016). However, a membrane with a higher thermal, chemical and mechanical stability would be needed for the purpose of expending membrane applications to aggressive media, such as acids and alkali solutions, in wastewater treatment, and industrial water treatment (Condom et al., 2004; Kermanpur et al., 2008; Skluzacek et al., 2007). It has been proved that ceramic membranes can resist a high temperature (up to 500 °C) and extreme pH-values (pH 1-14) (Benfer et al., 2001).

Ceramic membranes are made of inorganic, non-metallic materials, usually $Al_2O_3$, $TiO_2$ and $ZrO_2$, by the action of heating and subsequent cooling (Liu, 1996), which gives them superior chemical, thermal and mechanical properties. Historically, ceramic membranes are less used than polymer-based membranes, due to their higher fabrication costs and lower packing densities (Yacou et al., 2013; Gitis and Rothenberg, 2016). Fortunately, the question of cost, which is central to the future of ceramic membranes, is gradually being resolved by industrial R&D (Gitis and Rothenberg, 2016). Some modules, e.g., have been developed to increase the packing density of ceramic membranes, such as multi-channel monoliths and hollow fibre configurations. For hollow-fibre mem-

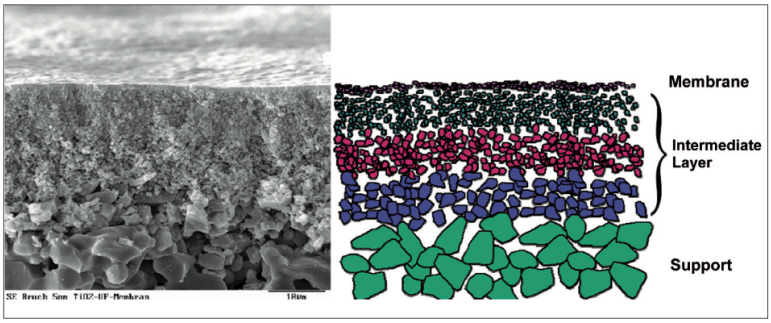


Figure 1.1: Typical structure of a ceramic membrane

branes, the packing density can be greater than 1000 $m^2/m^3$ (Bhave, 2012). Ceramen Corporation (Waltham, MA) has already commercialized ceramic membranes deposited on honeycomb monolith coerdierite supports with the packing density up to 800 $m^2/m^3$ (Goldsmith, 1991). The ceramic membranes with a multi-channel tubes configuration can have a packing density as large as 782 $m^2/m^3$ (Lee et al., 2015).

### 1.1.2. Structure and Characteristics of Ceramic Membranes

Ceramic membranes can be categorized according to their (i) structure, (ii) material, (iii) production method, and (iv) applications. Depending on their structure, membranes can be defined as dense (non-porous) or porous membranes. Dense membranes are usually made for hydrogen and oxygen separation. For porous membranes, there are a variety of membranes according to their pore size difference, namely microfiltration (MF), ultrafiltration (UF), nanofiltration (NF) and reverse osmosis (RO) membranes in a descending order of pore size.

Ceramic membranes are generally a porous membrane consisting of several layers with different properties and composites. As Figure 1.1 shows (Duscher, 2013), usually, a ceramic membrane has a ceramic support layer, e.g. consisting of $Al_2O_3$, onto which several porous separating layers, often silica, alumina or zirconia (Gobina, 2006) (Ku et al., 2008), with decreasing pore sizes, are deposited, until the desired pore sizes are reached. The supporting sub-layer serves as a substrate giving the selective layer enough mechanical stability and strength (Strathmann et al., 2011).

Ceramic NF membranes are often asymmetric, layered structures composed of a thin selective top layer which plays the main role in separating particles and dissolved compounds, and a pile of ceramic support layers below the top layer.

### 1.1.3. The Application of Ceramic Membranes in Water treatment

Ceramic membranes can be applied in the following fields: the food and beverages, biotechnology, chemical industry, pharmaceuticals' production and recovery and recycling (Schäfer et al., 2005), where they can compete with polymeric membranes in performance and economics. Since the study is designed to explore the membrane separation in the wastewater treatment field, we would mainly introduce the application of ceramic membranes on liquid separation.

UF and MF membranes have a pore size usually ranging from several nanometers to several micrometers. Therefore they are intrinsically used to separate colloidal particles or large molecular weight solutes. As the rejection of solutes is determined by the pore size, pore size distribution of the membranes and surface interactions between membrane surface and solvent/solutes. Examples of successful commercial-scale plants that use MF/UF ceramic membranes include purifying and concentrating valuable components such as enzymes and fermentation broths in biotechnology industries (Sondhi et al., 2003), and treatment of highly oily wastewater and degreasing baths (Majewska-Nowak, 2010). In contrast, ceramic membranes are much less commonly used in water and wastewater treatment, such as for the production of drinking water and treatment of municipal wastewater.

RO rejects all the solutes, including monovalent ions, while the NF membrane can only reject multi-valent ions. Today, ceramic RO/NF membranes are not commercially available, due to the high cost and and low packing density of ceramic membranes (Li, 2007). And their extremely low permeability is also an existing problem for their application in water treatment.

## 1.2. Fabrication of Ceramic Membranes

### 1.2.1. Support Layer

A generalized procedure for preparation of composite ceramic membranes is: (1) preparation of the ceramic powder paste (suspension); (2) shaping of the ceramic powder into the desired geometry; (3)heat treatment to consolidate the particles, including calcination and sintering; (4)thin layer coating through dip-coating, sol-gel or CVD and ALD processes, which is illustrated in Figure 1.2. The methods that are often used to give the slurry or paste the desired shape are: slip casting or tape casting, extrusion and pressing (Li, 2007; Gitis and Rothenberg, 2016).

#### Casting

Slip casting is probably one of the most commonly used methods in ceramic membrane preparation. In this method a well-mixed powder paste or suspension (slurry) is poured into a porous mould, and the solvent of the suspension is extracted via capillary forces into the pores of the mould (Tiller and TSAI, 1986). The particles of the suspension then

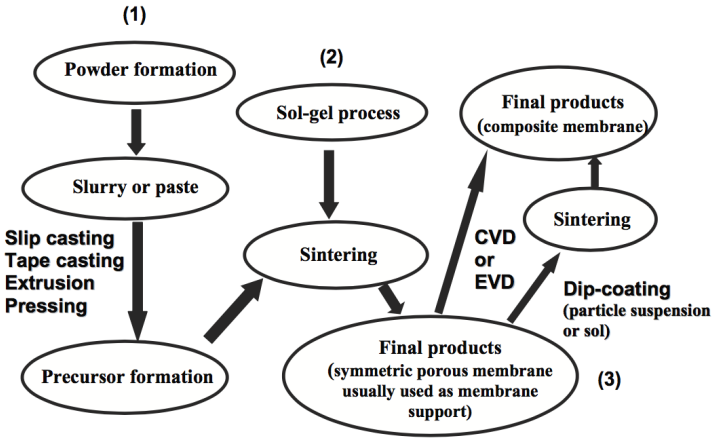


Figure 1.2: A general schematic review on fabrication procedure of composite ceramic membranes (Li, 2007)

consolidate on the surface of the mould to form a layer of particles or a layer of gel. The pore size and pore distribution are mainly dependent on the particle size of the used powders used in suspension preparation.

Tape casting is a another common way for producing flat ceramic membranes and discs (Gitis and Rothenberg, 2016). The process consists of a stationary casting knife, a reservoir, a moving carrier and a drying zone. The powder suspension is poured into the reservoir behind the casting knife, and the carrier to be cast upon is set in motion. The gap between knife blade and carrier determines the thickness of the membrane.

#### Extrusion

Extrusion is a productive method for producing ceramic membranes. Most ceramic tubular support for the fabrication of inorganic membranes is produced by extrusion (Li, 2007). The process is simple. A viscous paste is compacted and shaped by forcing it through a nozzle and then transformed into a stable shape in a coagulation bath by spinning (Isobe et al., 2006).

#### Pressing

Pressing is commonly used in making flat membranes or discs on lab-scale. An applied force is used to consolidate particles into a dense layer in a special press machine which holds the pressure higher than 100 MPa. The diameter of the products ranges in a few centimemters and the thickness is roughly 0.5 mm (Li, 2007).

### 1.2.2. Intermediate and Top Layers

The fabrication methods mentioned above are capable of making ceramic membranes with pore sizes > 1 $\mu$m. When the applications require a membrane with pore size less

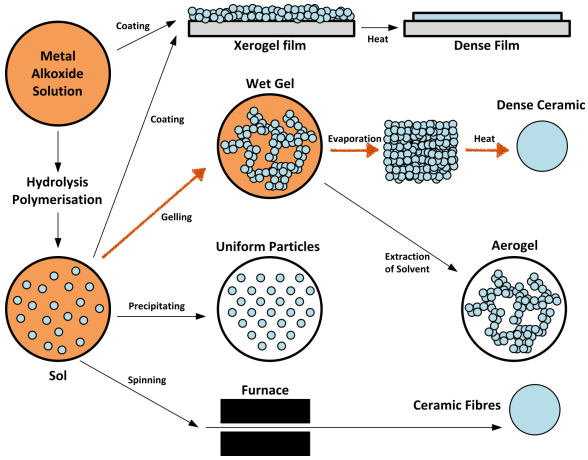


Figure 1.3: Schematic representation of the different stages and routes of the sol-gel technology

than 1 $\mu$m , additional intermediate layers and a top membrane layer are needed (Gitis and Rothenberg, 2016).

### Sol-Gel Method

The Sol-gel method is involved when membranes with pore size ranges of 1-100 nm are required (Das and Maiti, 2009). The Sol-gel method is a wet-chemical technique widely used for the fabrication of materials starting from a colloidal solution, often metal alkoxide or salts. The colloidal solution acts as a precursor, which gradually evolves towards the formation of gel-like phase system (Uche, 2013). The fraction of particles in the colloidal solution is usually too low to recognize gel-like properties, therefore a subsequent drying process, to remove the remaining liquid is required. Afterwards, a thermal treatment, often sintering, is necessary to enhance the mechanical strength and structure stability. As Figure 1.3 illustrates, there are several approaches for applying the sol-gel method, among which the route with the orange arrow represents the process described above.

### Atomic Layer Deposition

Atomic layer deposition (ALD) is an alternative technique for depositing thin films for a variety of applications. It is a self-limiting gas-phase thin film technology where atomic scale thin layers of metals, polymers and many other materials are grown on the support substrate. ALD is based on binary reactions' sequences where two precursors, which are strictly separated, adsorb on the pore wall and have a surface reaction with a previously adsorbed precursor (Li et al., 2012). Between each surface reaction, there is a purge step with inert gas to remove the unreacted precursors and by-products (Marichy et al., 2012). Figure 1.4 shows a complete cycle of ALD process, consisting of two dose steps and two

1

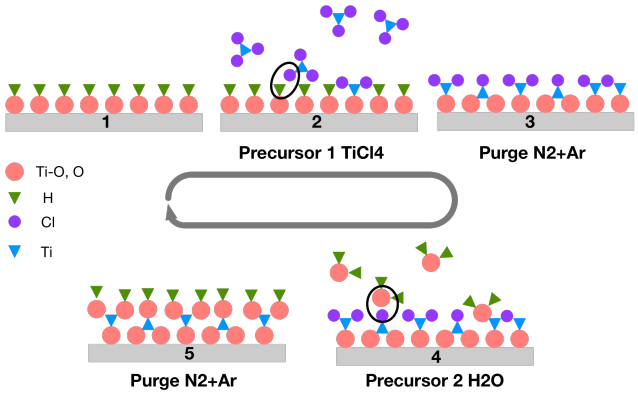


Figure 1.4: A general schematic draw of one complete ALD cycle

purge steps.

- **Thermal ALD** Thermal ALD is referred to when the surface reactions are thermally-driven. The thermal ALD can be operated at elevated temperatures (typically 150-350 °C).

- **Plasma-Enhanced ALD** , shortened as PEALD, came to light in 1992, when De Keijser and Van Opdorp of the Philips Research Laboratories in Eindhoven published a report on atomic layer deposition of GaAs using H radicals (De Keijser and Van Opdorp, 1991). However, the method was not developed until the end of 1990s, when semiconductor industries began being interested in this ALD method. In contrast to thermal ALD, plasma ALD, also referred to plasma enhanced ALD (PEALD), provides the needed energy by generating a large amount of radicals which contain high reactivity. The radicals, generated at low temperature, prevent high heat flux during deposition, and therefore allow for more freedom in processing parameters and for a wider range of deposition materials Profijt et al. (2011). The commonly used radicals are oxygen (O) radicals, nitrogen radicals and hydrogen radicals (H).

## 1.3. Thesis Research Framework

### 1.3.1. Problem Statement

Ceramic tight UF membranes are gaining more and more attention due to their inherent advantages compared with polymeric membranes (Mori et al., 1998). Their high thermal, mechanical and chemical stability make them much more applicable in treating e.g. corrosive wastewater (Van Gestel et al., 2002; Burggraaf and Cot, 2009). However,

due to the small pore size of tight UF membranes, which gives them a greater selectivity, there are some problems appearing:

- Permeability drops. It is commonly known that a higher selectivity usually results a smaller permeability (Spillman, 1995; Sengupta and Sirkar, 1995). The flux can be increased by decreasing the membrane thickness. However, lowering the thickness of a given membrane would increase the risk of forming defects which in turn decrease the selectivity of the membrane.

- Membrane fabrication process require more accurate control of the membrane structure and thickness. With the smaller pore size, membranes become more sensitive to micro crack. Even a small single crack of a few micrometers allowing a convective flow potentially neutralize the permselective properties of a membrane area many orders of magnitude its size (Burggraaf and Cot, 2009).

According to the problems mentioned above, it is urgent to find a thin-film deposition technology which would prepare defect-free or defect-poor thin separation layers without sacrificing too much permeation and make the fabrication process more controllable and standardized. The Sol-gel method, which has been widely used in making ceramic membranes, seems not to be able to make tight UF and NF membranes with this stable quality and a good reliability. Lin et al. has reported significant variations in the thickness of the permselective layer along the membrane length of commercial, tubular $Al_2O_3$ membranes (Lin et al., 1994). ALD has been suggested as a promising modification technology to produce a better separation layer, but not much results about deposition on tight UF ceramic membranes with ALD were found. The innovative technology has been tested in some studies (Kim and Oh, 2014), where was found that pore size tuning by ALD is limited to the top layer of the selective layer. Due to the smallest pore size in the top layer, the resistance of the liquid passing through membranes mainly comes from the top filtration layer. Therefore, the permeability can be reserved as much as possible if the pore-size-narrowing is limited in a very shallow depth of the membrane (Li et al., 2012).

### 1.3.2. Research Question

To solve the problems stated above, the following research questions were formulated:

- What is the coating depth of thermal ALD and PEALD on ceramic tight UF membranes? Since the resistance in composite membranes mainly comes from the top filtration layer, the shallower the coating depth is, the less resistance the ALD coating would create. Less resistance growth represents a less loss of permeability, which is the main goal of this study.

- What is the permeability and Molecular weight cut-off (MWCO) of the coated tight UF ceramic membranes and what is the difference between PEALD and thermal ALD? MWCO is a commonly used way to test the selectivity of a porous membranes. It defines the molecular weight above which more than 90 % of each size of molecules can pass the membrane.

### 1.3.3. Outline of Thesis

In this thesis, the research on three sizes of tight UF ceramic membranes, which originally had a MWCO of 2300, 6200 and 10100 Da respectively, were addressed in different aspects.

In Chapter 1, an overview of the development of ALD is given, with particular emphasis on its application on ceramic membranes.

In Chapter 2, the materials and methods used in the study are described. In addition, the advanced technique for characterizing membranes will be treated.

The results from all experiments and analyses on them is the topic of Chapter 3.

In the last chapter (Chapter 4), conclusions, obtained from the comparison of thermal ALD and PEALD, and some corresponding recommendations, are put forward.

# 2

# Methodology

## 2.1. Substrate Membranes

Ceramic tight UF membranes, provided by Inopor company, were used as substrates membranes for ALD coating. All membranes were in disc shape with a diameter of 90 $mm$ and thickness of 2.5 $mm$, while the effective filtration surface area was 0.0056 $m^2$, corresponding with an effective diameter of 0.084 $m$.

The ceramic tight UF membranes from Inopor GmbH, Germany, had different series, namely 2K series, 7K series and 10K series, with a separation layer made of zirconia ($ZrO_2$) or alumina ($Al_2O_3$). The support layer is made of $Al_2O_3$.

The claimed properties of the received membranes from Inopor company are described in Table 2.1. However, great variations in actual MWCO has been observed. Therefore a set of characterization tests were conducted to confirm the properties of the membranes.

Table 2.1: Properties of substrate membranes from TAMI industries and Inopor company*

| Supplier | Series | Material | Pore Size (nm) | Porosity | Cut-off (Da) |
|---|---|---|---|---|---|
| **TAMI** | 3K | $TiO_2$ | 2.2** | | 3000 |
| | 8K | $TiO_2$ | 3.3** | | 8000 |
| **Inopor** | 2K | $ZrO_2$ | 3 | | 2000 |
| | 7K | $Al_2O_3$ | 5 | 30%-50% | 7500 |
| | 10K | $Al_2O_3$ | 10 | | 20000 |

*: specification from manufacturer

**: estimated using Eq. (4.3) (Van der Bruggen and Vandecasteele, 2002)

## 2.2. Atomic Layer Deposition (ALD)

### 2.2.1. ALD system



Both thermal ALD and plasma ALD were performed in a single ALD system, Oxford ALD system (FlexAL®). The O radicals, used in the plasma ALD process, was generated by a built-in remote inductively coupled plasma (ICP) source operated at 200W and 13.56 MHz. In this remote configuration, continuous plasma operation was found to have a negligible contribution to substrate heating (Kubala et al., 2009). Both in thermal ALD and the plasma process, $TiCl_4$ was used as first precursor for coating $TiO_2$ onto substrate membranes. In thermal ALD, water was used as second precursor while in plasma ALD $O_2$ plasma was used. $N_2$ and Ar, as inert gases, played the role of delivering precursors and purging the system between reaction steps. The exposure level of $TiCl_4$ was controlled by alternating the dose time. $N_2$ and Ar gases were fed at a constant rate of 100 sccm and 150 sccm, respectively.

### 2.2.2. Wafer Coating

#### Growth rate measurement

The reason of performing wafer coating before membrane coating is that measuring the Growth rate per cycle (GPC) on a porous membrane was not technically feasible and therefore a planar wafer was provided as an alternative to monitor the GPC of each coating process.

A wafer, also called a slice or substrate, is a thin slice of semiconductor material, such as a crystalline silicon, used in electronics for the fabrication of integrated circuits and in photovoltaics for conventional, wafer-based solar cells (Laplante, 2005). The wafer serves as the substrate for many micro fabrication process steps, such as doping or ion implantation, etching, deposition of various materials, and photolithographic patterning. Silicon wafers used in this study, as the name indicated, are merely thin slices of a large single crystals of silicon that are formed by a process known as *Czochralski growth* (Mitchell, 2004; Wolf and Tauber, 1986).

Silicon wafers with a diameter of 100 $mm$ and thickness of 525 $\mu m$ were used in this study to deposit $TiO_2$ on it. Due to the flat geometry of the wafer surface, the growth of oxidization film after deposition was measurable by ellipsometry technology. Ellipsometry is an optical measurement technique for investigating the dielectric properties of thin films. It measures the changes in polarized light upon light reflection and light transmission on a sample and models the thickness by using a dielectric function model (Fujiwara, 2007). In this study, wafers coated with oxidized materials were measured by ellipsometer (M-2000F, J.A.Woollam Co. Inc., USA) using Cauchy model. A five-points scanning pattern was applied when measuring the thickness of the wafer, as Figure 2.1 shows.

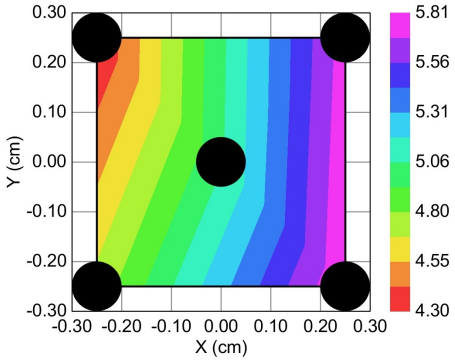


Figure 2.1: Five-points scanning pattern of measuring thickness of coated wafer by using Ellipsometer

The thickness of native oxide layer ($SiO_2$) on the surface of each silicon wafer was measured by the ellipsometer as a reference. After coating of metal oxides, the thickness of the as-deposited films was measured again, deducting the thickness of the original $SiO_2$ layer. Therefore the growth-per-cycle (GPC) of each coating could be measured (Shang et al., 2017).

#### Wafer coating in two positions

In order to explore the potential application of the ALD method in the fabrication of tubular ceramic membranes in future work, we put the wafer upside down and left the wafer a few millimeters from the chamber ground to let the gas diffuse well, as in Figure 2.2. If the precursor, which is in the gas phase, can diffuse effectively in a confined space as in an open space like the planer wafer or plate-shape ceramic membrane, then it can be expected that the technology is also technically applicable for tubular ceramic membranes.

### 2.2.3. Membrane Coating

In order to distinguish the coating material and the original material of a membrane, the metal oxides to be used in the coating process were chosen accordingly. The Inopor membranes (2K, 7K and 10K series), which are mainly made of $Al_2O_3$, were coated with $TiO_2$. Therefore two recipes (Table 2.2) were involved in the ALD coating process. One of them was for thermal ALD, and the other one was for PEALD. The dose time of $TiCl_4$ in PEALD was 70 ms, which was shorter than that in thermal ALD. The reason for this difference is that the PEALD recipe gave the same GPC no matter the dose time of $TiCl_4$ was 70 ms or 3 s.

All membranes were coated with corresponding metal oxides via 20 cycles of ALD. Each recipe was pretested on wafers to obtain the GPC on planar substrates. The whole

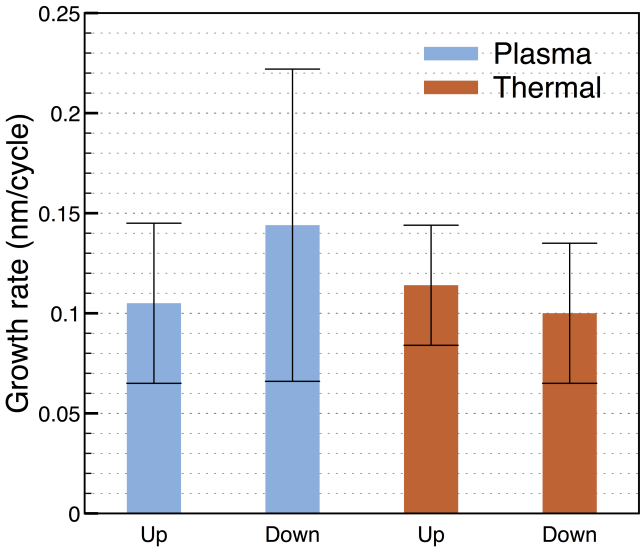


Figure 2.2: Wafer coated in two positions (the right is normal position with front side upside; the left is a reversed position with the other side towards up; the blue square with a cross inside depicts the five-points scanning position)

process was operated at a constant temperature of 180 °C for both thermal ALD and PEALD. The reaction chamber and delivery line was always preheated to the target temperature to prevent temperature jumps during the coating process.

A complete cycle of coatings is as follows: Firstly, the system was vacuumized and preheated to target conditions; then the first precursor was delivered into the reaction chamber and reacted with the substrate within a time period, followed by a purge step with inert gases; after purging, the second precursor was dosed and reacted with the substrate for a fixed period of time, also followed by a purging step. Except the pumping and preheating steps, the dose-purge-dose-purge cycle was repeated until the total cycles was reached. After the last cycle, the system was evacuated to a base pressure.

As Table 2.3 shows, 2K1, 7K1 and 10K1 were coated by thermal ALD, while 2K2, 7K2 and 10K2 were coated by PEALD. The rest of the membranes were treated with the same process except for the coating procedure and were used as blanks.

## 2.3. Filtration Experiment

### 2.3.1. Filtration Set-up

The filtration experiments were conducted in the Waterlab at TU Delft, where a filtration system was installed. The system consists of two feed tanks of 50 L capacity each, a membrane unit and a circulation loop. The photo and schematic overview of this setup

Table 2.2: Recipes for ALD coating of $TiO_2$

| Thermal | | Plasma | |
|---|---|---|---|
| $TiCl_4$ dose | 3 s | $TiCl_4$ dose | 70 ms |
| $TiCl_4$ purge | 30 s | $TiCl_4$ purge | 30 s |
| $H_2O$ dose | 3 s | Plasma $O_2$ | 6 s |
| $H_2O$ purge | 30 s | Plasma purge | 6 s |



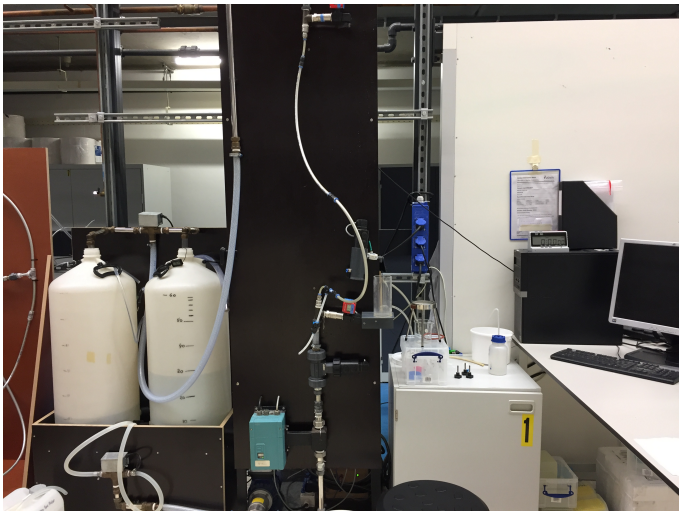

Figure 2.3: Photo of filtration set-up in lab

are shown in Figure 2.3 and Figure 2.4. A cross-flow with constant Trans-membrane pressure (TMP) of 3 bar was applied. Both the concentrate and permeates were fed back into the feed tank except for the samples' volume which was small compared to the feed water volume (< 2%).

### 2.3.2. Experimental Protocol

All membranes were firstly characterized by performing a permeability test and MWCO measurements, followed by chemical cleaning, where NaClO of 0.2% weight percent was used. After chemical cleaning, characterization was done again. The performances of the membranes in the permeability tests, before and after chemical cleaning, were compared. Chemical cleaning were repeated until the permeability got stable and then MWCO measurements were done after a series of permeability tests to determine the final MWCO of each membrane before they proceeded to the ALD coating procedure. The characteristics of all substrate membranes are shown in Table 2.3.

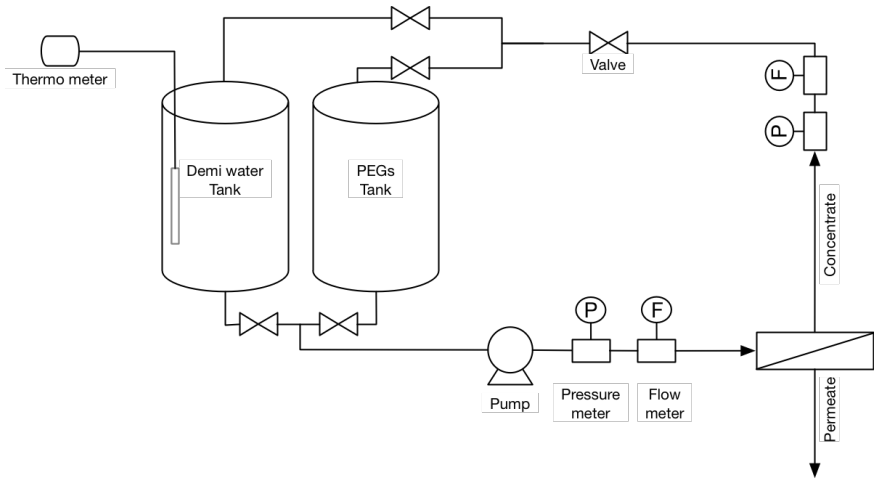


Figure 2.4: Schematic map of filtration experiment

### 2.3.3. Permeability

Pure water filtration performance was examined by temperature-corrected permeability. Demineralized water was filtered through the substrate membranes at a constant TMP of 3 bar. Three samples were collected during a 140-minutes filtration experiment to determine water flux and feed water temperature was monitored. An increase in water temperature was observed, which could be a result of heat transfer from the cross-flow pump, and therefore a temperature-corrected permeability equation was used to account for the temperature changes, Eq. (2.1), (Shang et al., 2017),

$$L_{p,20°C} = \frac{J}{\Delta P} \cdot \frac{\eta_T}{\eta_{20}} = \frac{J \cdot e^{-0.0239 \cdot (T-20)}}{\Delta P} \tag{2.1}$$

where: $L_{p,20°C}$ – permeability at 20°$C$, $m^3/(m^2 \cdot s \cdot \text{bar})$
$J$ – measured membrane flux, $m^3/(m^2 \cdot s)$
$\eta_T$ – permeate viscosity at measured water temperature
$\eta_{20}$ – permeate viscosity at 20 °C
$T$ – measured water temperature, °C
$\Delta P$ – measured TMP, Pa

### 2.3.4. Molecular Weight Cut-off (MWCO)

MWCO is defined as the molecular weight (in daltons) of a tracer molecule which is retained by the membrane with 90%. A mixture of a Polyethylene glycols' (PEGs) solution with a concentration of 0.6 $g/L$ was filtered through the substrate membranes at room

Table 2.3: Life stories of all membranes

| Membranes | ALD Method | Coating material | Recipe* (Da) | Chemical Cleaning (hours) | SEM-EDX | BET |
|---|---|---|---|---|---|---|
| **2k1** | Thermal | $TiO_2$ | 1000-6000 | 150 | Yes | Yes |
| **2k2** | Plasma | | | | | |
| **2k3** | Blank | | | | | |
| **2k4** | Blank | | | ——— | | |
| **7k1** | Thermal | | | 210 | | |
| **7k2** | Plasma | | | | | |
| **7k3** | Blank | | | | | |
| **7k4** | Blank | | ——— | ——— | | |
| **10k1** | Thermal | | 4000-35000 | 36 | | |
| **10k2** | Plasma | | | | | |
| **10k3** | Blank | | | | | |
| **10k4** | Blank | | | | | |

*: recipes of PEGs for MWCO measurement

temperature and under constant TMP of 3 bar. The molecule weight of the PEGs' feed solution ranged from 1000 Da to 35000 Da. Different recipes were used, depending on the announced membrane cut-off (Table 2.3). Because the PEGs are non-charged, their rejection by the membrane is mainly the results of steric hinderance. It means that the PEGs that are larger than the MWCO of the membrane would be rejected while smaller ones could pass through the membrane. In each filtration test, both permeate and feed solution were sampled and also temperature was monitored.

To calculate the MWCO of the received membranes, the permeate and feed solution samples, which were only filtered by a 0.45 micrometer filter, were analyzed by a high-performance liquid chromatography system (HPLC, Shimadzu, Japan), equipped with a size exclusive chromatography columns (SEC, 5 $\mu m$ 30 Å , PSS Polymer Standards Service GmbH, Germany). SEC, also known as gel permeation chromatography or gel filtration chromatography, separates solids on the basis of molecular size.

Calibration was done to determine the relation between the elution time and molecular weight, similar to that shown in Figure 2.5. The peak height is linear to the concentration of a single molecule. Using a polynomial or power model to fit the data (molecule weight in function of elution time) gives a calibration curve, as Figure 2.6 shows, where each elution time corresponds to a specific molecular weight. With the calibration curve, the retention curve of a PEG with a certain molecular weight can then be plotted using

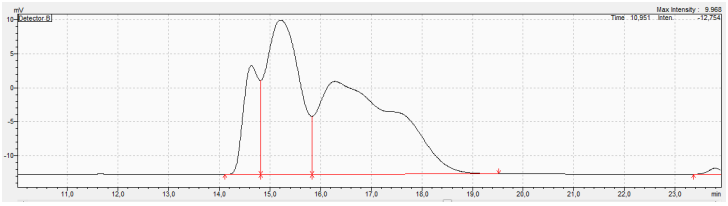

Figure 2.5: An example of elution peak results of PEGs from HPLC

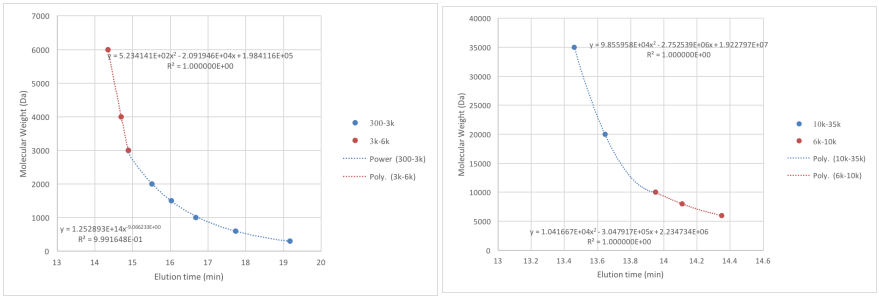


Figure 2.6: Calibration curve for PEGs from 300 to 35000 Da

Eq. (2.2) (Shang et al., 2017; Mulder, 1991). Furthermore, it was assumed that the pore size of the tight UF membranes follows a log-normal distribution (Van der Bruggen and Vandecasteele, 2002). Therefore, the experimental rejection curves were described by a log-normal model as function of MW and MWCO, given by Eq. (2.3) (Shirley et al., 2014; Van der Bruggen and Vandecasteele, 2002). Figure 2.7 gives an example of modeling results of MWCO from one analysis, where the grey dotted line represents the data obtained from the filtration test and the black line is the modelling result.

$$R_i(\%) = \frac{C_{i,\text{feed}} - C_{i,\text{permeate}}}{C_{i,\text{feed}}} \tag{2.2}$$

where: $R_i(\%)$ – retention of PEG molecule i, %
$C_{i,\text{feed}}$ – PEG concentration in feed solution, mg/L
$C_{i,\text{permeate}}$ – PEG concentration in permeate solution, mg/L

$$\sigma(\text{MW}_s) = \int_0^{\text{MW}_s} \frac{1}{S_{\text{MW}}\sqrt{2\pi}} \frac{1}{\text{MW}} \exp[-\frac{(\ln(\text{MW}) - \ln(\text{MWCO}) + 0.56S_{\text{MW}})^2}{2S_{\text{MW}}^2}] d\text{MW} \tag{2.3}$$

where: $\sigma(\text{MW}_s)$ – reflection coefficient, %
$S_{\text{MW}}$ – standard deviation of molecular weight retention, Da
MW – molecular weight cut-off, Da

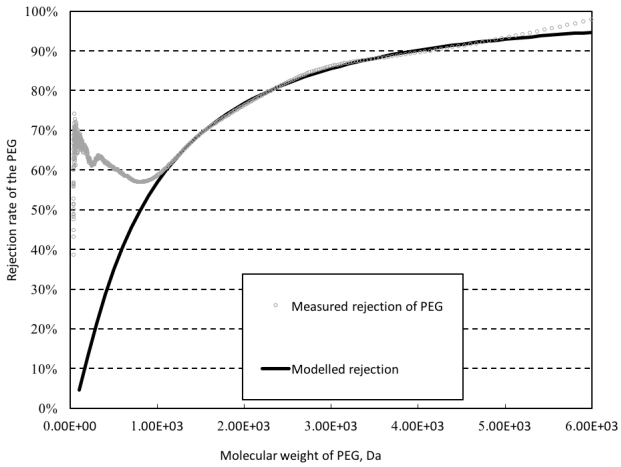


Figure 2.7: A typical graph of PEG rejection of ceramic NF membranes by log-normal distribution

### 2.3.5. Membrane Defects Calculation

Some defects were found in some studied membranes, and that was probably due to the inability of the fabrication method in making micro-pore-scale ceramic membranes. In order to make the results of the filtration performance comparable within studied membranes, a defect-correction model was built and applied both in MWCO and permeability. The principal idea of the defect-correction model was that the solutes which had a smaller size than the size of defect would all pass through the defect, but they would only partly pass through the membranes that are without any defects. The model is illustrated in Figure (2.8), and the complete calculation was done as below.

For any PEG ($i$ Da), given $R_{i0} = a\%$, $R_i = b\%$:

after adjustment, Eq. (2.2) can be written into:

$$1 - R_i = \frac{C_{i,\text{permeate}}}{C_{i,\text{feed}}} \tag{2.4}$$

While,

$$C_{i,\text{permeate}} = \frac{C_f \cdot (J - J_0) + C_f \cdot J_0 \cdot (1 - a\%)}{J} \tag{2.5}$$

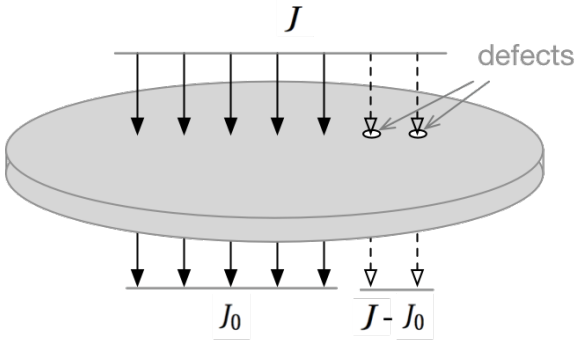


Figure 2.8: Schematic process of liquid passing through a membrane with defects

Substituting Eq. (2.5) into Eq. (2.4) gives Eq. (2.6),

$$1 - R_i = \frac{C_f \cdot (J - J_0) + C_f \cdot J_0 \cdot (1 - a\%)}{J \cdot C_f} \tag{2.6}$$

$$1 - b\% = (1 - d\%)(1 - a\%) + d\%$$

$$\longrightarrow a\% = \frac{b\%}{1 - d\%}$$

where: $J$ – total flux through membrane including defects, $m^3/(m^2 \cdot s)$
$J_0$ – flux through membrane without defects, $m^3/(m^2 \cdot s)$
$R_i$ – rejection of PEG ($i$ Da) in a membrane with defects, %
$R_{i0}$ – rejection of PEG ($i$ Da) in a membrane without defects, %
$d$ – defect of a membrane, %

After defect-correction, the corrected rejection of each PEGs for a membrane without defects was obtained, which was $a$% in Eq. (2.6) and then the rest of the calculation for MWCO was the same as mentioned beforehand (Eq. (2.2) and Eq. (2.3)). The flux was also corrected accordingly, following Eq. (2.7), and then the permeability were obtained combining Eq. (2.1) and Eq. (2.7).

$$J_{\text{corrected}} = J_{\text{measured}} \times (1 - d\%) \tag{2.7}$$

## 2.4. Characterization of Membrane Surface

### 2.4.1. Scanning Electron Microscope

Scanning Electron Microscope (SEM) is a type of electron microscope that can produce high-resolution images of a sample surface. By using SEM, the microstructure of studied membranes was observed and the thickness of top filtration layer was directly measured. Since the filtration layer significantly affect the performance of ceramic membranes, the

precise of measurement of filtration layer is important. With SEM technique, the image of the samples have a magnification of 15000x (7K series) and 35000x (2K and 10K series).

SEM produces high resolution images of a sample by scanning the surface with a beam of condensed electrons. The electrons strike the sample surface and interact with atoms in the sample, resulting in the release of various signals including secondary electrons (SE), back-scattered electrons, characteristic X-rays, light, absorbed current and transmitted electrons (Goldstein et al., 2012).

Due to the three condenser lenses installed alongside the beam pathway, the incident electron beam becomes so narrow and energetic that SEM micro graphs can have a large depth of field, yielding a characteristic three-dimensional appearance, useful for understanding the surface structure of a sample (Goldstein et al., 2012).

Among these various signals, the most common imaging mode collects low-energy (<50 $eV$) secondary electrons. In secondary electron imaging, or SEI, the secondary electrons are emitted from very close to the specimen surface as a result of interactions between energetic beam electrons and weakly bound conduction electrons (Streitwolf, 1959).

The cross-section structure of the membranes was analysed, before and after ALD coating, using a scanning electron microscope (SEM, FEI Nova NanoSEM 450, USA). Membranes were firstly coated with a thin film of gold (15 $nm$), by low-vacuum sputter coating techniques, in order to be electrically conductive. This coating is necessary because ceramic membranes, as a non-conducting specimen, collect electric charge when scanned by a beam of high-energy electrons. Accumulated charge in specimen exhibits a charging phenomenon which can result in a significant loss of material from the specimen and other image artifacts (Goldstein et al., 2012; Maissel and Glang, 1970). Membranes coated with a thin film of gold were then mounted rigidly to a specimen holder using carbon tape which also prevents the accumulation of electrostatic charge. The electron beam scans the specimen in a raster pattern and both positions of beams and signal detector contribute to the formation of surface image and surface topography (Reichelt, 2007).

### 2.4.2. Energy-Dispersive X-ray Spectroscopy

The composition and abundance of elements in samples were analysed using energy dispersive X-ray (EDX) analyzer (Ametek EDAX$^{TSL}$), which is coupled in a SEM-EDX system. In order to investigate the distribution of coating material in pores, the changes of $TiO_2$ abundance in pores before and after the ALD modification was analysed.

The cross sectional samples were scanned by a line scan pattern at 10 $kV$ accelerating voltage and 500 × magnification. The length of the scanning line drawn on each sample was approximately 1 to 2 $\mu m$ and normally 200 to 300 frames were taken.

The principle behind EDX technology is similar to that of SEM. EDX is suited for ana-

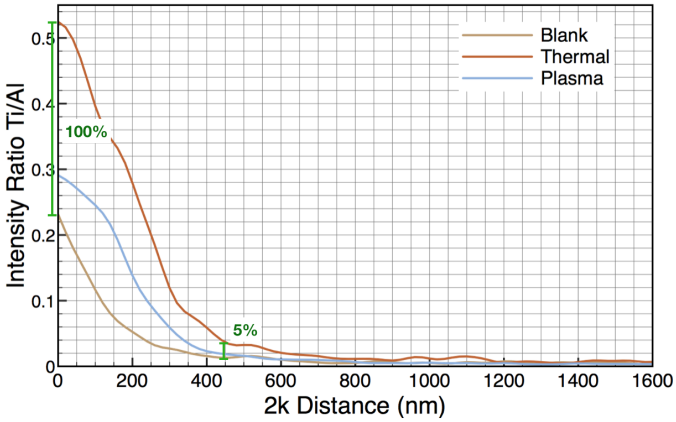


Figure 2.9: Schematic diagram of defined effective coating depth

lyzing the composition and abundance of elements. The principle is that electron beams not only react with atoms in samples, but also remove an inner-shell electron, resulting a vacancy in the electron shell. A higher-energy electron in the outer shell would, right after, fill the vacancy and release energy, which forms the characteristic X-ray (Goldstein et al., 2012; Russ, 2013).

### Effective Coating Depth

In order to make the results from the EDX measurements on different cross sections of membranes comparable, we define an effective coating depth ($\ell_c$) as the depth where the difference of element abundance between blank membrane and deposited membrane decreases to 5% of that at the surface. Figure 2.9 shows the schematic diagram of effective coating depth in thermal-coated 2K membrane.

# 3

# Results and Discussion

## 3.1. Thermal ALD vs PEALD

### 3.1.1. Growth Rate of Thin Film

The GPC on wafer in the case of thermal ALD was 0.025 nm/cycle. Ritala et al. (1993b) tested thermal $TiCl_4/H_2O$ process under different temperatures and found that the GPC is only 0.035 nm/cycle at 200 °C (Ritala et al., 1993b). When they changed the precursors to titanium tetraisopropoxide (TTIP) and $O_2$, the GPC was even lower than that with $TiCl_4/H_2O$, around 0.015 nm/cycle at 150 °C (Ritala et al., 1993a).

In PEALD process, $TiO_2$ thin film were deposited using $TiCl_4$ and plasma activated oxygen. The growth rate of $TiO_2$ on silicon wafers was 0.076 nm per cycle, as shown in Figure 3.1. This growth rate agrees well with the reported values of 0.06 – 0.07 nm/cycle at a temperature of 200 °C reported by Xie et al. (Xie et al., 2008). They also found that the GPC varied among different metal precursors. The GPC of $TiO_2$ using titanium tetraisopropoxide (TTIP) dropped to 0.04 – 0.05 nm/cycle. A GPC value of around 0.05 nm/cycle has also been reported for most PEALD using organometallic ligands (Lim et al., 2004; Xie et al., 2008). Kariniemi et al. (2012) reported a GPC of 0.05 nm/cycle at 150 °C for PEALD (Kariniemi et al., 2012), while Niskanen et al. (2007) obtained a GPC of 0.19 nm/cycle at 50 °C using TTIP as metal precursor (Niskanen et al., 2007).

In this study, the GPC during thermal ALD (0.025 nm/cycle) are lower than that obtained using PEALD (0.076 nm/cycle). This result has a good agreement with the data in the literature (Aarik et al., 2001; Matero et al., 2001; Ferguson et al., 2004).

### 3.1.2. Structural Characterization

Figure 3.2 presents the SEM micrograph of the cross sectional SEM image of membranes and the abundance ratio of elements obtained from the corresponding line-scan measurement. Table 3.1 summarizes the thickness of the filtration layer ($\ell_f$) and efficient coating zone ($\ell_c$), and Figure 3.3 depicts the efficient coating depth ($\ell_c$) in a bar graph for ease of comparison between thermal ALD and PEALD.

It can be clearly seen that in Figure 3.2 both in the case of thermal ALD and PEALD that the amount of Ti decreases gradually from membrane surface to deeper depths.

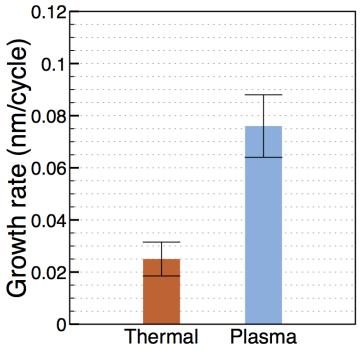


Figure 3.1: Growth rate of $TiO_2$ on wafers by PEALD and thermal ALD (Error bars represent standard deviation of a set of corresponding measurements)

The abundance of the deposited film along with the coating depth can be categorized as the character of conformality of deposition. A conformal thin film is a layer of film on a substrate with the same thickness everywhere along the interface. Since the ALD technology is mainly used in semiconductor or other metallic material industry, there is few literature reporting the data of $TiO_2$ deposition concerning conformality. Ritala et al. (1993a,b) found that the films of deposited $TiO_2$ at the shallow part of substrates were thicker and resulted in a thickness difference of up to 60 nm with 2000 reaction cycles at 600 °C (Ritala et al., 1993a,b). In some more recent publications, Kubala reported a ~ 24% decrease of thickness relative to the surface in a substrate with an aspect ratio of 9:1 (Kubala et al., 2009) and a decrease of ~ 37% in a substrate with aspect ratio of 3:2 (Kubala and Wolden, 2010). The aspect ratio of the substrate in the literature usually refer to the ratio of its depth to its width. Moreover, this phenomenon has also been observed in some deposition experiments of Ag and Ru. Kim et al. (2008) and Kim and Oh (2014) (Kim et al., 2008; Kim and Oh, 2014) found that the Ru deposition was limited to the top part of nanoscale via but did not give any detailed data. Kariniemi et al. (2012) observed only one micrometer deep of continuous Ag film growth in a trench with an aspect ratio of 10, which had an opening with a the width of 115 nm at the surface. (Kariniemi et al., 2012).

For thermal ALD, the conformality is determined by the transport of the precursor molecules into the hole (Gordon et al., 2003; Elam et al., 2003; Dendooven et al., 2009), while the amount of precursors transported throughout holes is limited by two factors, the flux available at the entrance of the hole and the exposure time (Gordon et al., 2003; Dendooven et al., 2010). If sufficient exposure time is not provided, the thickness profile is characterized by a slope of decreasing thickness, as shown in Figure 3.2.

In spite of the similar decreasing trend of thickness profile observed both in the case of thermal ALD and PEALD, they show a distinctive character in all the three sizes of

membranes. Membranes derived from PEALD always show a shallower coating depth than those that were derived from thermal ALD. Of the 2K and 7K membranes, the coating depth of thermal ALD was almost two times larger than the depth obtained with PEALD (Table 3.1). For the ease of comparison, Figure 3.3 summarizes the efficient coating depth of different membranes. For PEALD, the presence of radical recombination is in addition attributed to the loss of active particles (Kim et al., 2008; Kim and Oh, 2014). Radicals generated by the plasma generator not only deposit, but also recombine on the pore wall surfaces to form nonreactive molecules that desorb back into the plasma flux (Profijt et al., 2011). The main difference between thermal ALD and PEALD is that PEALD involves reactive species that not only undergo ALD reactions (as in thermal ALD), but also react with other radicals and species residing at the surface (Profijt et al., 2011). The mechanism of recombination of radicals has not been explored much, until recently that some authors tried to simulate and quantify the impact of surface recombination on the quality of deposited film (Knoops et al., 2010; Dendooven et al., 2009, 2010). In the model, They used two independent factors, reaction probability $s$ (also called sticking probability) and recombination loss probability $r$. Reaction probability involves the basic surface reactions occurring both in thermal ALD and PEALD, i.e., lingend exchange, dissociation, association, etc.. Recombination loss probability is defined as the possibility of loss of radicals due to recombination during deposition. The surface recombination probability is determined by species of radicals and the material of the surface with which the radical reacts with (Knoops et al., 2010). In Monte Carlo simulations, the same authors (Knoops et al., 2010; Dendooven et al., 2009, 2010) used a variety of combinations of $s$ (0.001-1) and $r$ (0-0.9) to represent different scenarios. Simulation results showed a great fit with their experimental data. When $r$ increased, the recombination effect became stronger and the conformality along the pores became poorer (Knoops et al., 2010). In our case, thermal ALD can be regarded as a process with a $r$ of zero. Therefore deposited film in the case of PEALD is thinner than that in the case of thermal ALD at the same depth. The values of $s$ and $r$ are dispersed in literature and reproduced in Table.B.1 and Table.B.2.

Most of the radicals probably recombine in this way to deeper parts of the membrane, resulting in a dramatically reduction of the flux of radicals and less deposition in the deeper pores (Knoops et al., 2010). It can be seen at Figure 3.2 that the starting point of PEALD is much lower than that of Thermal ALD, which indicates that the precursors which arrived at the substrate surface is much less in the case of PEALD. This is possibly because that some radicals are lost due to recombination on the way to the substrate surface.

In addition, the amount of $TiO_2$ deposited on the membrane pores by thermal ALD is larger than the amount deposited by PEALD, according to the area surrounded by the red line (thermal ALD) or blue line (PEALD) and the yellow line (blank line) in Figure 3.2.

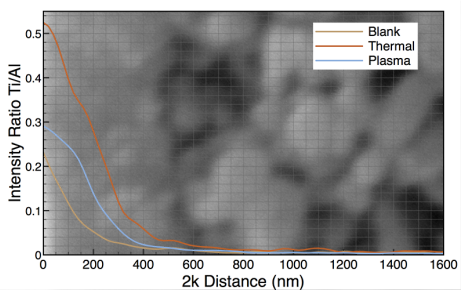


(a) 2K series

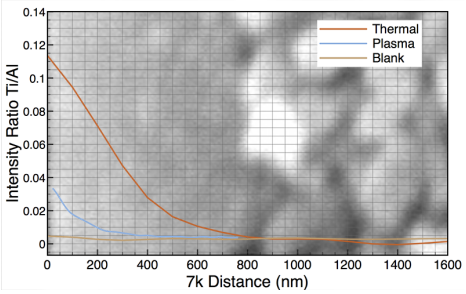


(b) 7K series

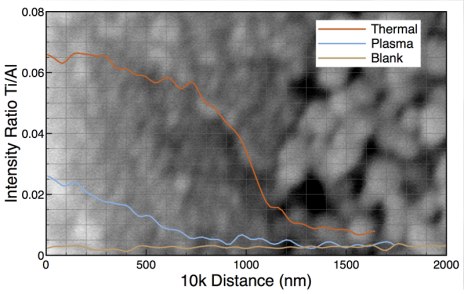


(c) 10K series

Figure 3.2: Ratio of abundance of Ti to Al of Inopor membranes measured in Line-scan analysis by EDX

Since part of radicals got lost due to recombination during diffusing into deeper pores, it is reasonable to assume that the total effective radicals those contributing to pore surface reaction were less in PEALD and so was the average thickness of deposited film. Hereby, the fact that thermal ALD always showed a higher deposition amount in each depth might be explained.

### 3.1.3. Filtration Performance

Table 3.2 and Figure 3.5 show the results of the filtration performance of the coated membranes obtained from the filtration experiments before and after ALD deposition. Since we mainly focused on the changes in the coated membranes, the data file of other membranes including blank membranes can only be found in Appendix A.1 and Appendix A.2. It can be observed from the Figure 3.5a, that the permeability dropped considerably after deposition except for the 10K2 membrane. The decrease trend is mainly induced by the $TiO_2$ deposition on the pore surface and thus the reduction of the membrane pore size. Meanwhile, with the loss of permeability, the rejection performance of all coated membranes was enhanced, as expected (Figure 3.5b). Although the permeability of the 2K membranes did not show much difference between the membranes derived from PEALD and from thermal ALD, overall it still can be concluded that a less loss

Table 3.1: Summary of results from EDX measurement

| **Membrane** | ALD type | $\ell_f$,nm | $\ell_c$,nm | Slope* |
|---|---|---|---|---|
| **2K1** | | 497±15 | 220 | $1.0 \times 10^{-3}$ |
| **7K1** | Thermal | 1003±111 | 610 | $3.6 \times 10^{-4}$ |
| **10K1** | | 1132±141 | 1460 | $5.3 \times 10^{-5}$ |
| **2K2** | | 437±21 | 120 | $7.5 \times 10^{-4}$ |
| **7K2** | Plasma | 750±226 | 320 | $1.1 \times 10^{-4}$ |
| **10K2** | | 1040±65 | 1255 | $2.8 \times 10^{-5}$ |

$\ell_f$: thickness of filtration layer, measured from SEM image
$\ell_c$: coating depth, estimated from EDX measurement (Figure 3.2)
Slope: the decreasing rate of deposited film thickness on pores (thickness profile)

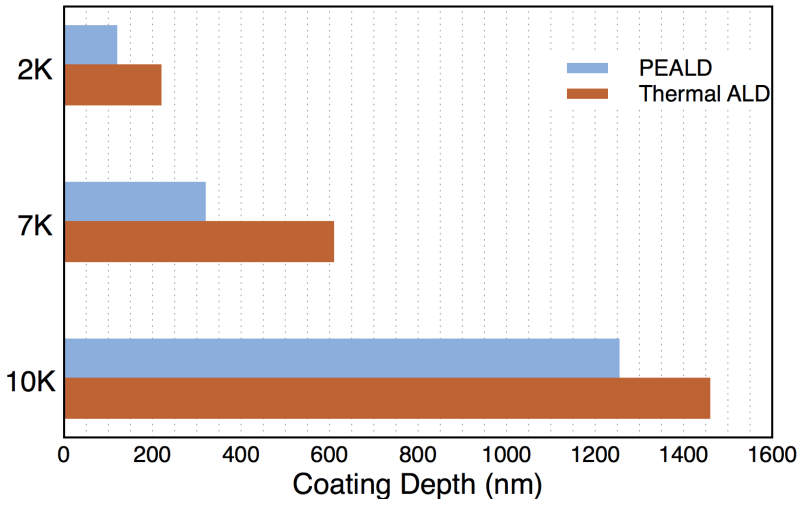


Figure 3.3: Efficient coating depth in as-deposited membranes after thermal ALD and PEALD

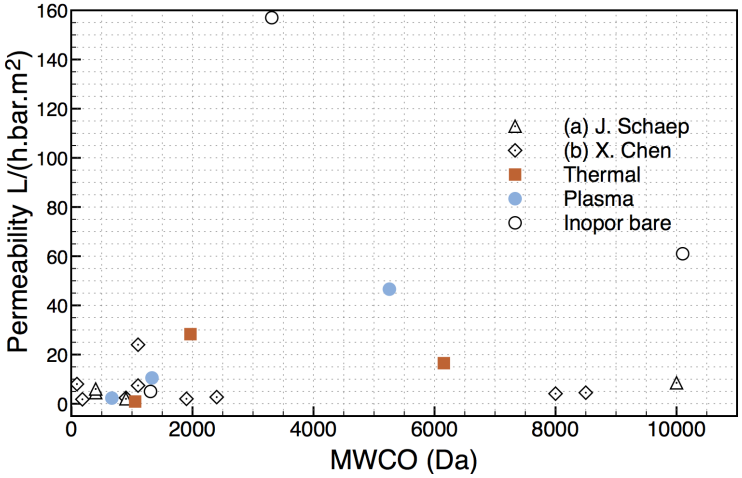


Figure 3.4: Permeability of membranes in some literature and our case. Notes: (a) values obtained from Schaep (Schaep et al., 1999); (b) values obtained from Chen (Chen et al., 2015).

of permeability was obtained when coating with PEALD. This is in agreement with the findings that the effective coating depth in the case of PEALD is smaller than in thermal ALD, as mentioned earlier. In principle, separation properties of a composite ceramic membrane, such as permeability, are usually controlled by the microstructure of the top separation layer, because the pore size in the top layer, compared with the pore size in support layers, is much smaller (Li, 2007). Therefore, the resistance in the support layer can be ignored and the resistance of the membrane can be assumed to be directly related to the pore size in top layer and the thickness of this layer. In a result, for PEALD, the resistance in the membranes is smaller due to the combination of smaller efficient coating depth and smaller pore size. Although, it should be pointed out that the coated membranes obtained from PEALD had a larger reduction of pore size within the coating part, which can be justified according to the reduction of MWCO, the permeability in the case of PEALD showed a smaller decline than that in thermal ALD, due to the positive impact of shallow coating depth on permeability.

Even though the pure water fluxes decreased sharply, they were still comparable with other ceramic NF membranes (Figure 3.4). Schaep et al. (1999) reported that a NF membrane with a MWCO of 4000 Da only has a permeability of 5 L/(m$^2$ h bar) and other membranes with a smaller MWCO even have lower permeabilities (Schaep et al., 1999). Other authors reported a permeability range from 1 to 4 L/(m$^2$ h bar) for membranes with a MWCO from 200 Da to 8000 Da (Qi et al., 2012; Van Gestel et al., 2008; Larbot et al., 1992, 1994; Baticle et al., 1997).

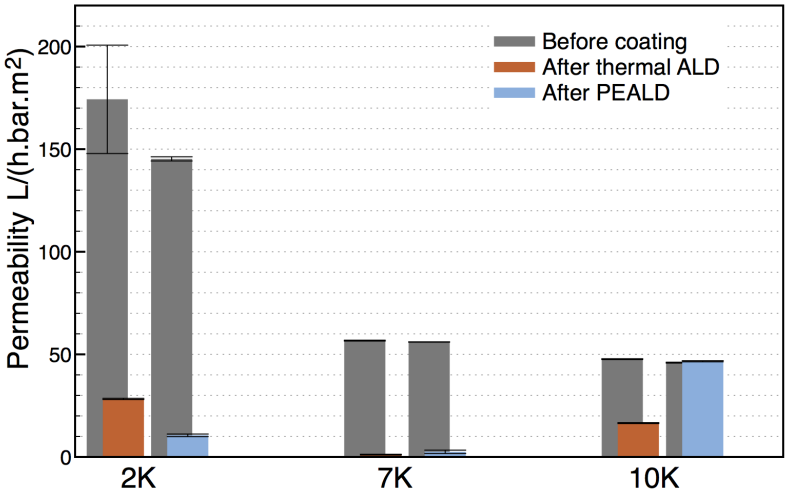


(a) Permeability

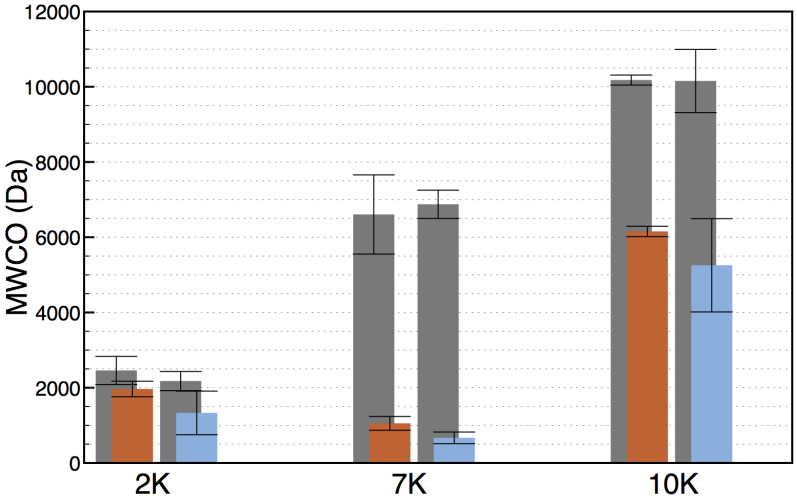


(b) Molecular cut-offs

Figure 3.5: The filtration performance of ALD-coated membranes after coating

Table 3.2: Filtration performance of as-deposited membranes

| Membrane | ALD type | Before | | | After | | |
|---|---|---|---|---|---|---|---|
| | | $L_p$ | MWCO | $D$ | $L_p$ | MWCO | $D$ |
| **2K1** | Thermal | 174.8 | 2458 | 1.99 | 28.3 | 1966 | 1.80 |
| **7K1** | | 43.1 | 6605 | 3.06 | 0.9 | 1052 | 1.37 |
| **10K1** | | 47.7 | 10178 | 3.70 | 16.5 | 6154 | 2.97 |
| **2K2** | Plasma | 145.3 | 2177 | 1.88 | 10.5 | 1330 | 1.52 |
| **7K2** | | 44.7 | 6875 | 3.12 | 2.3 | 667 | 1.12 |
| **10K2** | | 46.0 | 10153 | 3.70 | 46.6 | 5254 | 2.77 |

$L_p$: permeability in Eq. (2.1), L/(m$^2$ h bar)
$D$: estimated average pore size using Eq. (4.3), $nm$
MWCO: molecular weight cut-off, Da

## 3.2. Membranes With Different Pore Sizes

### 3.2.1. Performance

From Table 3.1 and Figure 3.3, it can be observed that the efficient coating depth increased with the MWCO (pore size). This is related to the transport mechanism of precursors during the ALD process. For ceramic membranes with a pore size at 2 nm or slightly larger, which is the situation of this study, the predominant mechanism is usually Knudsen diffusion (Li, 2007). Studies on membrane diffusion have clearly indicated that the diffusion coefficient is considerably influenced by the ratio of pore size to gas molecules (Beck and Schultz, 1970, 1972; Chantong and Massoth, 1983). Currie (1960) did some gaseous diffusion experiments in porous media and reported that the diffusion coefficient became greater when pore size increased, which means that in larger pores the resistance becomes smaller (Currie, 1960). Hence, in 10K membranes, the diffusion rate of the precursor is highest and the resistance is smallest. Therefore more precursors were able to diffuse to deeper parts of 10K membranes and had the chance to deposit on the pore wall. Accordingly, the 2K membrane had the smallest effective coating depth due to its most narrow pore size (Table.3.2).

It can be noticed that after the filtration experiments, some of the membranes suffered a higher drop in permeability than others, as well as higher reduction in MWCO. As a result, of these coated membranes, the 7K series obtained the highest percentual fall in permeability. In the meantime, the 7K membranes also showed a dramatic drop in MWCO, from 6700 Da decreasing to 800 Da, which is in agreement with its decline in permeability. However, the permeability of 7K after deposition is quite low compared to the values available in literature, as Figure 3.4 shows. The very possible reason is that the porosity of as-deposited 7K membranes dramatically decreased due to the deposition in

the pores. After deposition, 7K membranes had an average MWCO of 800 Da and average of pore sizes of around 1.2 nm. When compared with commercial 800 Da membranes, the coated 7K membranes do not show the superiority, because their porosity are much lower.

2K membrane also experienced a high permeability drop while the performance of rejection test of coated membrane did not match the permeability decline since the MWCO only decreased slightly. A possible explanation is that the pore size of the 2K membranes (1.9 nm) was so small that some of them were blocked during deposition. As a result, these blocked pores did not contribute to liquid transport anymore. In the meantime, these blocked small pores might not influence the pore size distribution or the entry pore diameter much and therefore did not reflect on the decrease in pore size. The reasons why the original permeability of the 2K series is so high is unknown because the fabrication procedure and the composition of the membrane has been made confidential.

Of the 10K membranes, the permeability of 10K2 (by PEALD) did not change while 10K1 (by thermal ALD) decreased from 47.7 L/(m$^2$ h bar) to 16.5 L/(m$^2$ h bar). This cannot be explained since in Table 3.1 it can be seen that the separation layer was coated entirely in both 10K1 and 10K2. The reason of the unchanged permeability of the 10K2 is still unknown but of the difference between 10K1 and 10K2 is possibly because that the amount of deposition in the separation layer is higher in the case of thermal ALD than that of the deposition during PEALD (Figure 3.2c). The greater amount of deposition further decreased the porosity of coated membranes and thus had a negative impact on permeability.

### 3.2.2. Defects Curing

Since the original membranes contained some defects, the evolution of these defects are also very important. From Table 3.3, it can be seen that there was no defect in the 2K membranes and the defects in the 7K and 10K membranes were reduced by 8.25% and 24.15% respectively after deposition. According to the mechanism of Knudsen diffusion in membrane pores, referring to the Section 3.2.1, the bigger pores get filled firstly and therefore the defects in the 10K membranes were completely cured while those in 7K membranes were partially cured.

## 3.3. Other Characterization

### 3.3.1. Potential application in Confined Geometry

In order to explore the potential application of ALD in the fabrication of tubular ceramic membranes, we put the wafer upside down and left the wafer a few millimeters from the chamber ground to let the gas diffuse well. The results are shown in Figure 3.6. From the

Table 3.3: Effect of ALD on membrane defects

| Membrane | Before | After | ALD type |
|---|---|---|---|
| **2K1** | 0.0% | 0.0% | Thermal |
| **2K2** | 0.0% | 0.0% | Plasma |
| **7K1** | 24.0% | 17.8% | Thermal |
| **7K2** | 20.2% | 9.9% | Plasma |
| **10K1** | 20.7% | 0.0% | Thermal |
| **10K2** | 27.6% | 0.0% | Plasma |



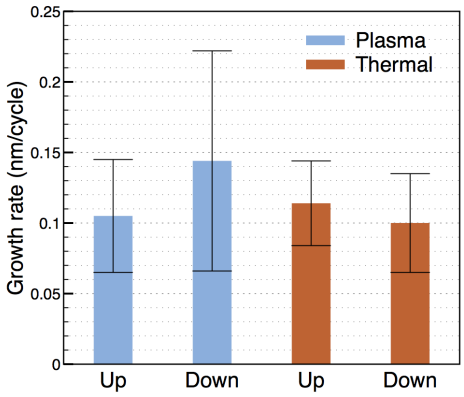


Figure 3.6: Growth rate of material on silicon wafer of front side and reverse side

results, it can be clearly seen that there was no observable difference between the two positions in both thermal ALD and PEALD. When the wafer was set upside down, the variation of GPC in the case of PEALD were higher than that in thermal ALD. What need to be considered is that, the space under the wafer when wafer was set upside down was very small, less than 1 m2. In terms of the application of ALD in tubular ceramic membranes, this is just a early step to explore the potential. So far, we can still assume that the precursors in the gas phase could have contact with the inner part of a channel in a tubular ceramic membrane, potentially not negatively influencing the coating possibilities for tubular membranes.

### 3.3.2. Uncertainty in Membranes Performance

All the membranes were characterized and chemically cleaned before they were coated in the ALD system. Therefore the data shown above with "before" label was obtained after the membranes were chemically cleaned several times. One of the reasons why we

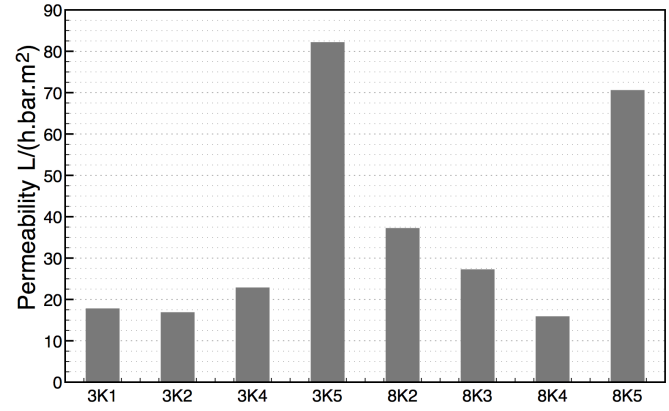


(a) TAMI membranes

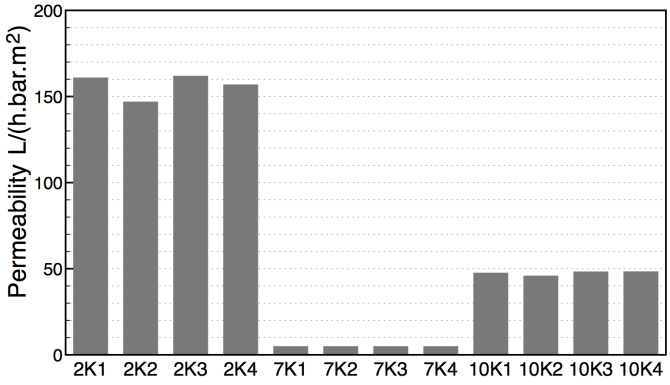


(b) Inopor membranes

Figure 3.7: Permeability of pristine membranes

performed these chemical cleanings is that the pristine membrane showed an inconsistent performance within the same series.

The permeability of both TAMI and Inopor pristine membranes are shown in Figure 3.7. It can be easily seen that TAMI membranes showed an inconsistent performance during the filtration test with demineralized water, even though they were claimed to be produced in one batch and be consistent in performance. Inopor membranes showed a more consistent performance during the water filtration experiment compared to those provided by TAMI.

From the results (Figure 3.8), however, it can be found that, except for the 2K series, the actual molecular cut-offs for pristine 7K and 10K series membranes, determined as around 1306 kDa and 10101 kDa, clearly deviated from the supplier's claimed values

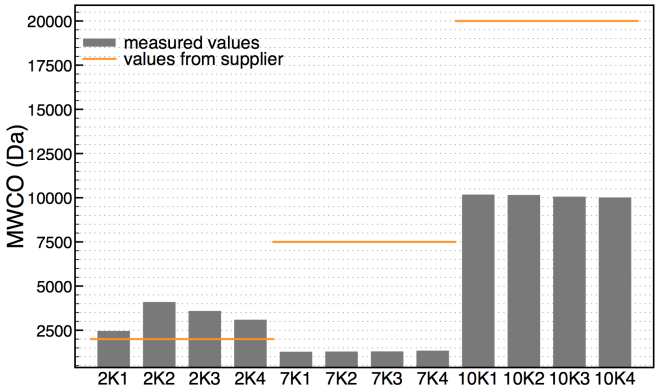


Figure 3.8: MWCO of pristine Inopor membranes

(7.5 kDa for 7K series and 20 kDa for 10K series). The cut-offs of the 7K series was even smaller than that of 2K series, which was beyond our expectation. The MWCO of 10K was highest, of 10000 Da, among the three series but was not so high as their claimed MWCO (20 kDa).

# 4

# Carman-Kozeny Model

## 4.1. Assumptions and Equations

The Carman-Kozeny relation, was used in this study to describe permeability, where the pores were assumed to be interstices between close-packed spheres (Figure 4.1) (Ergun, 1952; Seader et al., 1998; Sutera and Skalak, 1993). The Carman-Kozeny equation was originally developed by Kozeny in 1972 (McCabe et al., 1993) to calculate the pressure drop for laminar flow through a packed bed of solids (Kruczek, 2014), and was later combined with the Hagen-Poiseuille equation, to estimate the flux through a porous membrane, assuming that the pores may not be cylindrical and straight (Seader et al., 1998; Ergun, 1952). The Carman-Kozeny equation is depicted in Eq. (4.1).

$$J = \frac{\rho \varepsilon^3 \Delta P}{2(1-\varepsilon)^2 \tau a_v^2 \mu \ell} \tag{4.1}$$

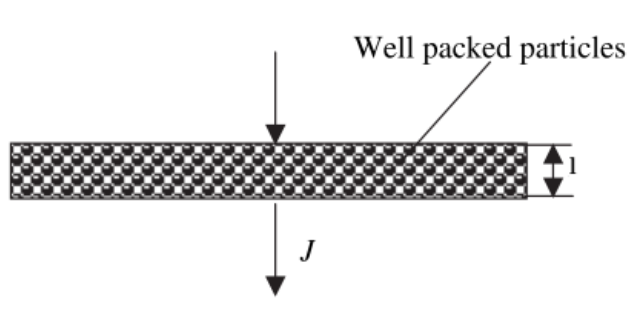


Figure 4.1: Ceramic membranes with well packed particles (Li, 2007)

where: $J$ – flux through membrane, $m^3/(m^2 \cdot s)$
$\rho$ – density of the fluid, $kg/m^3$
$\varepsilon$ – membrane porosity, -
$\Delta P$ – transmembrane pressure, pa
$\tau$ – tortuosity factor, -
$a_v$ – specific surface area, $1/m$
$\mu$ – viscosity of the fluid, pa·$s$
$\ell$ – layer thickness, $m$

In Eq. (4.1), $a_v$ is the specific surface area which has a relation with hydraulic diameter ($D$) of membrane pores, as Eq. (4.2) indicated (Seader et al., 1998).

$$a_v = \frac{4\varepsilon}{D \cdot (1-\varepsilon)} \tag{4.2}$$

Where,

$$D = 0.065 \times (\text{MWCO})^{0.438} \tag{4.3}$$

In Eq. (4.2) $D$ is hydraulic diameter of the membrane pores. Here we assumed that the hydraulic diameter of the pores was close to the average pore size of the membrane and therefore the pore size estimated from the measured MWCO (Eq. (4.3) of each membrane was used as the value for $D$ in this equation. All assumptions made for this model for estimating permeability are listed below:

1. The density and dynamic viscosity of the feed solution is assumed to be close to pure water in a condition of 25 °C and 101 325 Pa;

2. The hydraulic diameter of pores was close to the average pore size;

3. The tortuosity of membranes was estimated as 2.08 (Seader et al., 1998);

4. The resistance within the membrane is mainly in the top layer, which has the smallest pore size;

5. The porosity of all membranes before ALD was determined to be 0.55, which was the maximum value within the claimed range by the supplier (0.30-0.55). With chosen value 0.55, the model fits best with the measurement.

6. The porosity of the membranes after ALD were assumed to follow the relation in Eq. (4.4), in which the pore shape was assumed to be a sphere, and the number of pores ($n$) were assumed to be constant during ALD treatment, leaving the change of porosity only related to the change of diameter of the sphere (i.e. pore size).

Table 4.1: Parameters for Carman-Kozeny equation

| Fluid | | | Membranes | | |
|---|---|---|---|---|---|
| viscosity $\mu$ | pa· s | 0.00089 | porosity $\varepsilon$ | - | 0.55 |
| density $\rho$ | kg/m3 | 1000 | tortuosity $\tau$ | - | 2.08 |

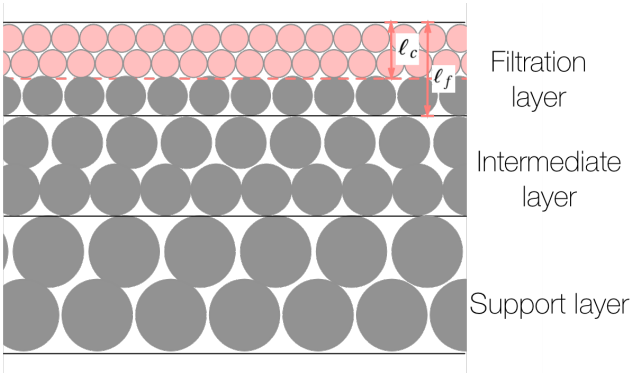


Figure 4.2: Two-layer structure in filtration layer of ceramic membrane after coating

$$\varepsilon_i = \frac{\text{void volume}}{\text{total volume}} = \frac{n \cdot \frac{\pi D_i^3}{6}}{V_{\text{total}}}$$
$$\longrightarrow \frac{\varepsilon_{\text{before}}}{\varepsilon_{\text{after}}} = \left(\frac{D_{\text{before}}}{D_{\text{after}}}\right)^3 \tag{4.4}$$

The values of the parameters presented above are given in Table 4.1 at a condition of 25 °C and 101 325 Pa.

### 4.1.1. Two-Layer Model

A two-layer model was created to represent the structure of the filtration layer of the membranes after ALD coating, as drawn in Figure 4.2. Since part or entire filtration layer was coated by coating process, the pore size in the coated region reduced accordingly. In order to mimic the structure of the membranes after ALD coating, the coated part and part below coating depth were treated separately. The pore size and porosity in the coated region changed to $D_{\text{after}}$ and $\varepsilon_{\text{after}}$ , while the rest part of the filtration layer ($\ell_f - \ell_c$) still have the same pore size, $D_{\text{before}}$, as before. The pore size of the membranes both before and after ALD coating was obtained by using Eq. (4.3), and the porosity after ALD coating was obtained by using Eq. (4.4). The resistance in the coated part ($R_c$) and part below the coated part ($R_{f-c}$) were summed to a total resistance ($R_{\text{total}}$) and then the total permeability ($J_{\text{total}}$) was calculated as in Eq. (4.5) and Eq. (4.6).

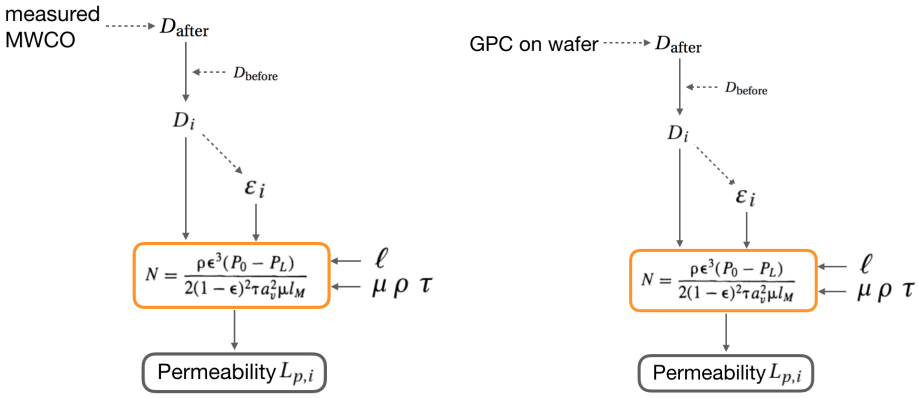


(a) Using MWCO (method 1)

(b) Using GPC on wafer (method 2)

Figure 4.3: Schematic view of Carman Kozeny model procedure

$$J = \frac{\Delta P}{\mu R} \longrightarrow R = \frac{\Delta P}{J \cdot \mu} \tag{4.5}$$

In the two-layer model, the total flux of deposited membrane can be calculated by first calculating the permeability of each layer independently and then adding the resistance in two layers (Eq. (4.6)).

$$\begin{cases} R_c = \frac{\Delta P}{J_c \cdot \mu} \\ R_{f-c} = \frac{\Delta P}{J_{f-c} \cdot \mu} \\ R_{\text{total}} = R_c + R_{f-c} \end{cases} \longrightarrow J_{\text{total}} = \frac{\Delta P}{\mu R_{\text{total}}} = \frac{J_c \cdot J_{f-c}}{J_c + J_{f-c}} \tag{4.6}$$

## 4.2. Procedure

The modeling process is depicted in Figure 4.3. The two methods, used in estimating the pore size of membranes, only have the difference on the method of calculating the pore size, leaving the rest of the calculation the same (Figure 4.3).

Firstly, the original pore size of the studied membranes were determined by the measured MWCO, which is named as $D_{\text{before}}$. After ALD deposition, the pore size, $D_{\text{after}}$, was calculated by using MWCO (method 1) or GPC on wafer (method 2). Then the pore size of the membranes after each single cycle was calculated by interpolating between $D_{\text{before}}$ and $D_{\text{after}}$. Finally, the corresponding porosity was calculated by using Eq. (4.4).

## 4.3. Model Results

The model result of method 1 and method 2 are shown in Table 4.2 and Table 4.3 respectively. With method 1, except the extremely high permeability of 2K membranes prior to

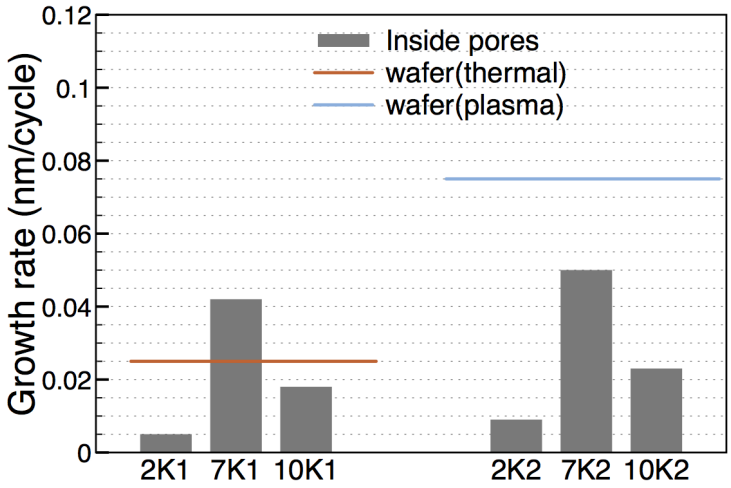


Figure 4.4: Growth rate of $TiO_2$ inside pores by PEALD and thermal ALD (Error bars represent standard deviation of a set of corresponding measurements)

ALD coating process, the rest of data fits well into the model. For 7K and 10K series, the data shows a good matching, which indicates that the original assumptions of porosity and tortuosity, estimation of pore size and filtration layer thickness works well with each other. The two-layer model seems thus to be a good assumption. While with method 2, the calculated permeability deviated a lot from the measured permeability. The reason why the modelled permeability was much smaller than the measured ones is that, we assumed the growth rate in pores was the same as the growth rate on wafers. However, the calculated growth rate (Eq. (4.3)) appeared to be much smaller than that on wafers (Figure 4.4). This leads to an overestimation of pore reduction in the calculation of method 2.

## 4.4. Model Sensitivity

Sensitivity analysis was conducted to investigate the influence of different starting porosity on membrane permeability. Figure 4.5 shows the relationship between the pore size and membrane permeability with different porosity. All the parameters, except porosity, used in this analysis are kept as the same to the ones used in model. As seen in Figure 4.5, when pore size increases, the discrepancy in permeability between different porosity becomes larger. Therefore when pore size is 2.70 nm (10K membranes), the discrepancy in permeability between porosity of 0.55 and 0.30 can be as high as 24.28 L/($m^2$ h bar). When porosity is fixed, the different formulas of estimating the pore sizes can also make a difference. There is already some literature reporting and compar-

Table 4.2: Model results of permeability from applying Carman-Kozeny equation by using MWCO (Method 1)

| | Before coating | | | After coating | | |
|---|---|---|---|---|---|---|
| | $\varepsilon^{*a}$ | $L_p$ | $L^*_{p,\text{model}}$ | $\varepsilon^{*b}$ | $L_p$ | $L^*_{p,\text{model}}$ |
| 2K1 | 0.55 | 174.8 | 26.5 | 0.41 | 28.3 | 20.7 |
| 2K2 | 0.55 | 145.3 | 27.1 | 0.29 | 10.5 | 17.7 |
| 7K1 | 0.55 | 43.1 | 31.3 | 0.05 | 0.9 | 0.9 |
| 7K2 | 0.55 | 44.7 | 43.3 | 0.03 | 2.3 | 0.6 |
| 10K1 | 0.55 | 47.7 | 40.4 | 0.28 | 16.5 | 13.4 |
| 10K2 | 0.55 | 46.0 | 43.9 | 0.23 | 46.6 | 10.4 |

*: estimated using Carman-Kozeny equation (Seader et al., 1998)
$*a$: assumed starting porosity
$*b$: estimated porosity using Eq. (4.4)
$L_p$: measured permeability in filtration test

Table 4.3: Model results of permeability from applying Carman-Kozeny equation by using GPC on wafer (Method 2)

| | Before coating | | | After coating | | |
|---|---|---|---|---|---|---|
| | $\varepsilon^{*a}$ | $L_p$ | $L^*_{p,\text{model}}$ | $\varepsilon^{*b}$ | $L_p$ | $L^*_{p,\text{model}}$ |
| 2K1 | 0.55 | 174.8 | 26.5 | 0.07 | 28.3 | 1.7 |
| 2K2 | 0.55 | 145.3 | 27.1 | 0.00 | 10.5 | -11.24 |
| 7K1 | 0.55 | 43.1 | 31.3 | 0.19 | 0.9 | 6.53 |
| 7K2 | 0.55 | 44.7 | 43.3 | 0.00 | 2.3 | 0.0 |
| 10K1 | 0.55 | 47.7 | 40.4 | 0.21 | 16.5 | 8.37 |
| 10K2 | 0.55 | 46.0 | 43.9 | 0.00 | 46.6 | 0.01 |

*: estimated using Carman-Kozeny equation (Seader et al., 1998)
$*a$: assumed starting porosity
$*b$: estimated porosity using Eq. (4.4)
$L_p$: measured permeability in filtration test

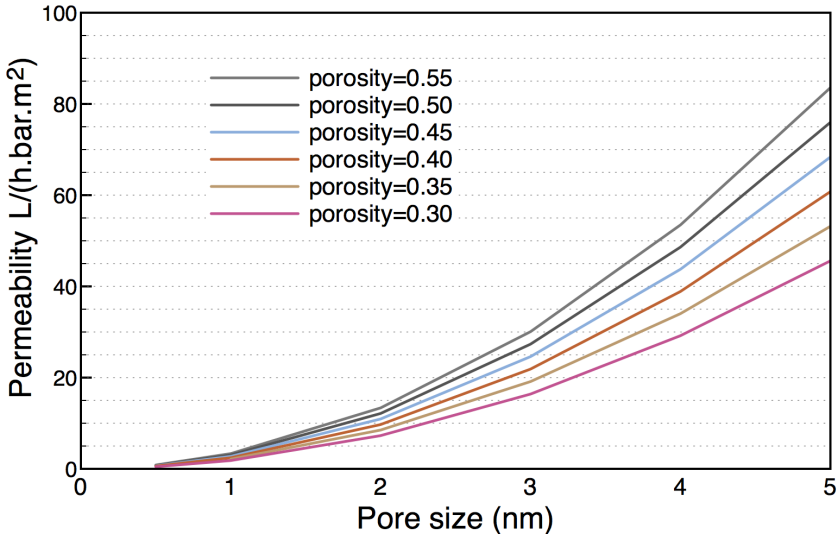


Figure 4.5: Sensitivity analysis of Carman Kozeny model

ing the different results by using different formulas and there are discrepancy between them (Van der Bruggen et al., 1999; Lin and Burggraaf, 1993). By applying one of the formula mentioned as Stokes diameter in literature, the estimated pore size was 0.79 nm for original 7K1 membrane, having a MWCO of 6605 Da. This result is much smaller than that obtained in this study, which was 3.06 nm. If 7K1 membrane has a porosity of 0.55 as we assumed before, the permeability of it can be 25 L/(m$^2$ h bar) or 5 L/(m$^2$ h bar) respectively, when the pore size is estimated as 2.79 nm and 0.79 nm.

## 4.5. Limitation

When Eq. (4.1) is employed for calculation of either the permeability or pore size, it contains much uncertainty because of the introduction of the membrane surface porosity and tortuosity. Two different types of characterization methods for the porous membranes can be distinguished: structure-related parameters and permeation-related parameters (Mulder, 1991). The former is about the determination of pore size, pore size distribution, top layer thickness and porosity while the latter is related to actual separation parameters using solutes that are partly retained by the membrane. Both the parameters obtained from the filtration experiment, carried out in this study, namely permeability and MWCO, are permeation-related parameters. It is usually hard to get the real pore geometry and some assumption have to be made beforehand. Although the configuration of pores in studied membranes does not strictly follow the close-packed-pattern or even might deviate dramatically from it, the model results, as discussed be-

fore, still gave some information about the membrane properties which can be used as a first estimate in determining possible application field (Mulder, 1991).

It should be pointed out that in two-layer model, we divided the filtration layer into two parts according to the calculated efficient coating depth, while in reality, the clear boundary does not really exist. The thickness of deposited film might decrease gradually from surface. And therefore there is some uncertainty when applying this model to calculate permeability. In addition, the good match of model results (method 1) and measured results does not necessarily mean that any single of these parameter is correct or close to the real value.

# 5

# Conclusions and Recommendations

## 5.1. Conclusions

The main objective of this study was to compare two types of atomic layer deposition (ALD) methods, namely thermal ALD and plasma-enhanced ALD (PEALD), for coating of thin films on ceramic ultrafiltration (UF) membranes. In this study, ceramic tight UF disc membranes with a diameter of 90 mm were used as the substrates. The performance of the studied membranes, consisting of permeability and the molecular weight cut-off (MWCO), was examined in this study. In addition, the effective coating depth of the coated membranes was calculated by analyzing the element abundance in the coated membranes. How the effective coating depth reflect on the membranes performance was also included. The following conclusions can be drawn from the experiments and analyses reported in previous chapters:

1. Performance of coated membranes
    - A clear decline in MWCO, measured by PEGs' rejection, and loss of permeability were observed in membranes coated by either thermal ALD or PEALD as compared to the original substrate membranes.
    - The decreases in MWCO, observed during the experiments, were proved to be caused by the narrowing of pore size.
    - The narrowing of pore size caused a decrease of porosity, which further resulted in a declined permeability. In addition, the pore loss due to pore blocking might also cause the loss of permeability.
2. Structure of coated membranes
    - The deposited film was not homogeneous along the pore wall and the amount of deposited material in the pores decreased towards the deeper parts of the separation layer of the membrane.
    - A more shallow coating depth was obtained by PEALD, which gave as-deposited membranes a better MWCO, while having less permeability loss than those coated by thermal ALD.

- Both thermal ALD and PEALD can partly or even totally cured the defects present in the substrate membranes with an original MWCO of 7K and 10K.

3. Characteristics of both thermal ALD and PEALD
   - Precursors diffuse more easily in bigger pores, which explains why the largest tested 10K membranes have the deepest effective coating depth.
   - When a wafer for testing the growth rate of deposition, was put upside down, the precursors ($TiCl_4$ and $H_2O$ for thermal ALD, $TiCl_4$ and $O_2$ plasma for PEALD) in the gas phase reacted with the surface as they did in the situation when the wafer was set in normal up position. This indicates that the methods could also be used for the coating of tubular membranes.
4. Carmen Kozeny model
   - The Carmen Kozeny model fitted the measurements data in the right order of magnitude. The model showed that the pore size suffered a great drop during deposition which also led to the decrease in porosity.
   - Since the Carman Kozeny model fitted well with the measurements data, it is therefore recommended to be used to calculate the permeability of ALD-coated ceramic membranes, and to testify the relationship between porosity, pore size of membranes and properties of liquids.



## 5.2. Recommendations and Future Study

From the research the following experimental recommendations and suggestions for future study are extracted:

- When using ALD or PEALD to narrow the pore sizes of ceramic membranes to a targeted pore size, it is recommended to select a membrane with a pore size near to the range of the target membrane, since the porosity would decrease considerably if the initial pore size (MWCO) is far from the target pore size. This is basically due to the restricted number of pores in the substrate membranes of higher initial MWCO.
- The coating conformality should be further studied on tubular ceramic membranes using ALD. In this study, we explored the diffusivity of precursors in confined geometry, and the result gave a positive signal to further study the films growth and conformality of deposited film on tubular ceramic membranes.
- Since we only used a fixed plasma exposure time in this study, it would be appealing to investigate the effect of different exposure times on the growth kinetics and

conformality in ceramic tight UF membranes with certain pore sizes. In the study by Dendooven et al. (2010) and Kariniemi et al. (2012), different exposure times were tested, and it was found that with a shorter exposure time, the conformality became poorer and the effective coating be more shallow, indicating that the loss of permeability during coating would probably be less.

# A

# Figures

A

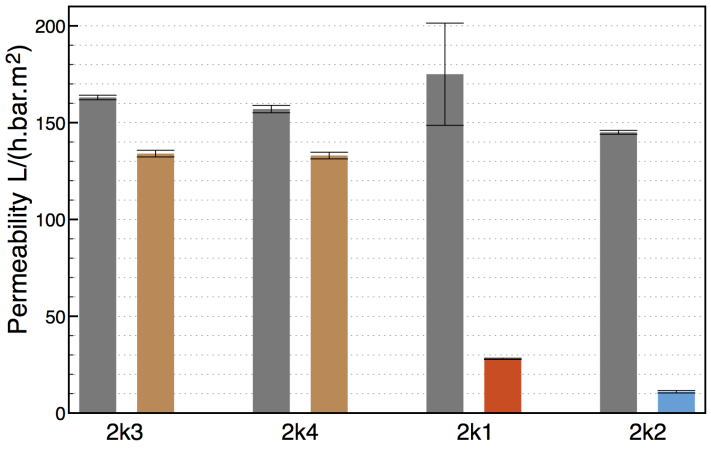


(a) 2K series

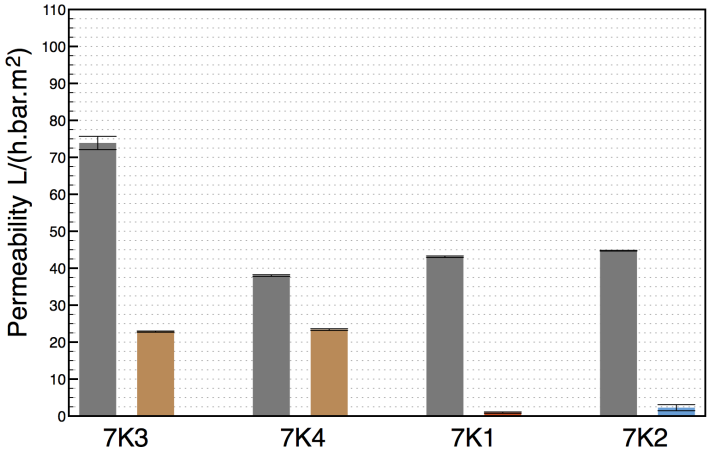


(b) 7K series

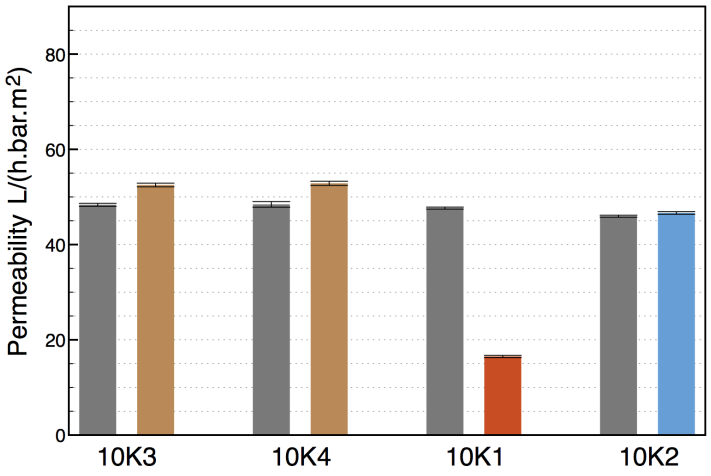


(c) 10K series

Figure A.1: Permeability of Inopor membranes before and after ALD

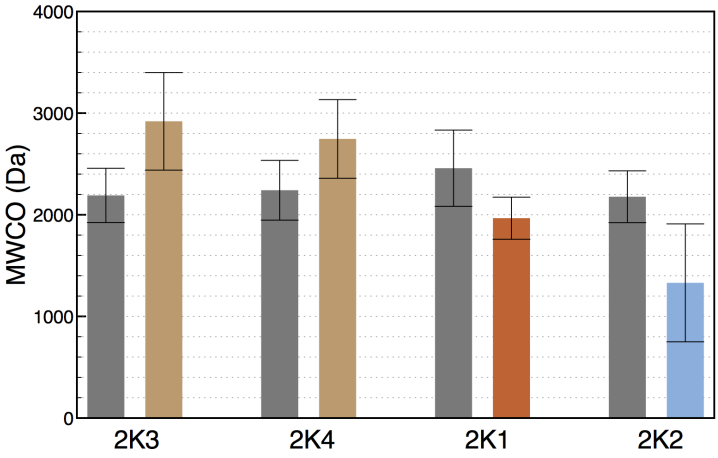


(a) 2K series

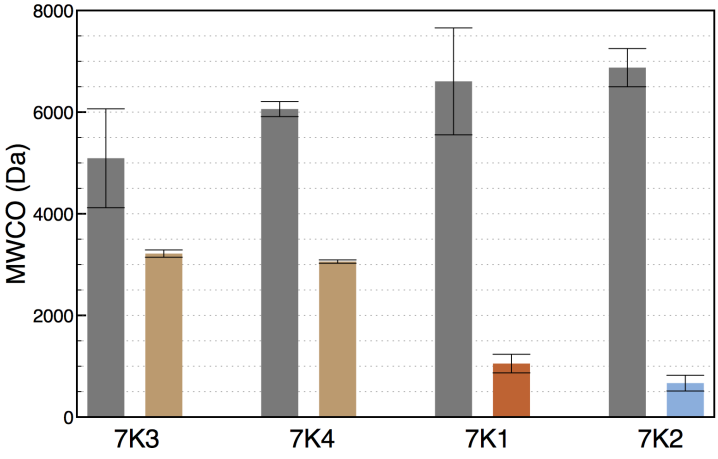


(b) 7K series

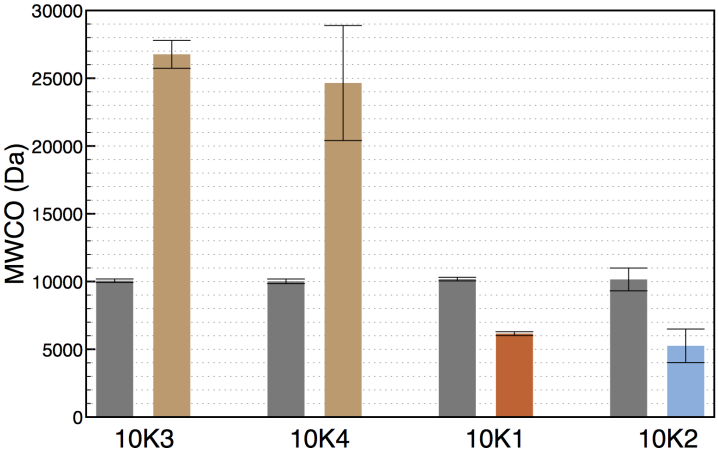


(c) 10K series

Figure A.2: MWCO of Inopor membranes before and after ALD

# B

# Tables

B

Table B.1: Reaction probabilities *s* for several precursors and reactants (including some related to plasma processes) as reported in the literature. The accuracy is indicated when available.

| Step | Species | Deposited material | Reaction probability | References |
|---|---|---|---|---|
| **Precursor** | $Al(CH_3)_3$ | $Al_2O_3$ | 0.001 | (Elam et al., 2003) |
| | $Al(CH_3)_3$ | $Al_2O_3$ | 0.026 | (Kim et al., 2007a) |
| | $Al(CH_3)_3$ | $Al_2O_3$ | 0.1 | (Dendooven et al., 2009) |
| | $Al(CH_3)_3$ | $Al_2O_3$ | 0.1-0.9 | (Prechtl et al., 2003) |
| | $Hf(NEtMe)_4$ | $HfO_2$ | 0.03-0.6 | (Rose et al., 2010) |
| | $Ti(NMe_2)_4$ | $TiO_2$ | 0.02±0.005 | (Rose and Bartha, 2009) |
| | $Ti(O^iPr)_4$ | $TiO_2$ | 0.04-0.1 | (Kim et al., 2007b) |
| | $Cp^*Ti(OMe)_3$ | $TiO_2$ | 0.01 | (Rose et al., 2010) |
| | $TiCl_4$ | TiN | 0.006±0.002 | (Greer et al., 2003) |
| | $ZnEt_2$ | ZnO | 0.007 | (Elam et al., 2003) |
| | $SiCl_4$ | $SiO_2$ | $10 \times 10^{-8}$ | (Elam et al., 2003) |
| **Reactant** | $H_2O$ | $Al_2O_3$ | 0.01-0.1 | (Prechtl et al., 2003) |
| | $O_3$ | $Al_2O_3$ | 0.001-0.01 | |
| **Plasma** | O | $Al_2O_3$ | 0.1-0.9 | (Prechtl et al., 2003) |
| | H | TiN | 0.0003±0.0001 | (Greer et al., 2003) |
| | N | TiN | 0.01±0.002 | |

Table B.2: Surface recombination loss probabilities $r$ for H, N and O radicals on various material surfaces as reported in the literature. The accuracy is indicated when available.

| Radical | Surface | Recombination probability | Reference |
|---|---|---|---|
| **H** | Silica | 0.00004±0.00003 | (Kim and Boudart, 1991) |
| | Alumina | 0.0018±0.003 | (Tserepi and Miller, 1994) |
| | Pyrex | 0.0058±0.0018 | (Wood and Wise, 1961) |
| | Stainless steel | 0.032±0.015 | (Tserepi and Miller, 1994) |
| | Silicon | 070±0.10 | (Abrefah and Olander, 1989) |
| | Titanium | 0.35 | (Wood and Wise, 1961) |
| | Aluminum | 0.29 | |
| | Nickel | 0.20±0.09 | (Tserepi and Miller, 1994) |
| | Copper | 0.14 | |
| | Gold | 0.15±0.05 | (Wood and Wise, 1961) |
| | Palladium | 0.07±0.015 | |
| | Platinum | 0.03 | |
| **N** | Silica | 0.0003±0.0002 | (Kim and Boudart, 1991) |
| | Stainless steel | 0.0063 | |
| | Silicon | 0.0016 | (Knoops et al., 2010) |
| | Aluminum | 0.0018 | |
| **O** | Silica | 0.0002±0.0001 | (Kim and Boudart, 1991) |
| | Pyrex | 0.000045 | |
| | Aluminum oxide | 0.0021 | |
| | Zinc oxide | 0.00044 | (Greaves and Linnett, 1959) |
| | Ferric oxide | 0.0052 | |
| | Cobalt oxide | 0.0049 | |
| | Nickel oxide | 0.0089 | |
| | Cupric oxide | 0.043 | |

B

Table B.3: Permeability and MWCO of all membranes and comparison with estimated permeability

| | Before coating | | | After coating | | |
|---|---|---|---|---|---|---|
| | **MWCO** | $\mathbf{P_{measured}}$ | $\mathbf{P^*_{modelled}}$ | **MWCO** | $\mathbf{P_{measured}}$ | $\mathbf{P^*_{modelled}}$ |
| 2K1 | 2458 | 174.8 | 26.5 | 1966 | 28.3 | 20.7 |
| 2K2 | 2177 | 145.3 | 27.1 | 1330 | 10.5 | 17.7 |
| 2K3 | 2190 | 163.1 | 20.2 | 2919 | 134.1 | 20.2 |
| 2K4 | 2241 | 156.6 | 26.1 | 2746 | 132.5 | 26.1 |
| 7K1 | 6605 | 43.1 | 31.3 | 1052 | 0.9 | 0.9 |
| 7K2 | 6875 | 44.7 | 43.3 | 667 | 2.3 | 0.6 |
| 7K3 | 5092 | 72.9 | - | 3216 | 22.8 | - |
| 7K4 | 6060 | 38.0 | 29.4 | 3059 | 23.4 | 29.4 |
| 10K1 | 10178 | 47.7 | 40.4 | 6154 | 16.5 | 13.4 |
| 10K2 | 10153 | 46.0 | 43.9 | 5254 | 46.6 | 10.4 |
| 10K3 | 10059 | 48.4 | 50.3 | 26763.0 | 52.5 | 50.3 |
| 10K4 | 10015 | 48.4 | 40.7 | 24647.0 | 52.9 | 40.7 |

*: estimated using Carman-Kozeny equation (Seader et al., 1998)

Table B.4: Thickness of filtration layers and efficient coating depth, $nm$

| **Membrane** | $\ell_f$ | $\varepsilon_{\text{before}}$ | $D_{\text{before}}$ | $\ell_c$ | $\varepsilon_{\text{after}}$ | $D_{\text{after}}$ |
|---|---|---|---|---|---|---|
| **2K1** | 497±15 | 0.55 | 1.99 | 220 | 0.41 | 1.80 |
| **2K2** | 437±21 | 0.55 | 1.88 | 120 | 0.29 | 1.52 |
| **2K3** | 589±86 | 0.55 | 1.89 | - | - | 2.14 |
| **2K4** | 466±98 | 0.55 | 1.91 | - | - | 2.08 |
| **7K1** | 1003±111 | 0.55 | 3.06 | 610 | 0.05 | 1.37 |
| **7K2** | 750±226 | 0.55 | 3.12 | 320 | 0.03 | 1.12 |
| **7K4** | 990±83 | 0.55 | 2.95 | - | - | 2.19 |
| **10K1** | 1132±141 | 0.55 | 3.70 | 1460 | 0.28 | 2.97 |
| **10K2** | 1040±65 | 0.55 | 3.70 | 1255 | 0.23 | 2.77 |
| **10K3** | 900±57 | 0.55 | 3.68 | - | - | 5.65 |
| **10K4** | 1110±128 | 0.55 | 3.67 | - | - | 5.45 |

$\ell_f$: thickness of filtration layer, measured from SEM image
$\ell_c$: coating depth, estimated from EDX measurement (Fig. 3.2)
$\varepsilon_{\text{before}}$, $D_{\text{before}}$: porosity and pore size of filtration layer before coating
$\varepsilon_{\text{after}}$, $D_{\text{after}}$: porosity and pore size of coated layer within filtration layer

# Bibliography


Aarik, J., Aidla, A., Mändar, H., and Uustare, T. (2001). Atomic layer deposition of titanium dioxide from ticl 4 and h 2 o: investigation of growth mechanism. *Applied Surface Science*, 172(1):148–158.

Abrefah, J. and Olander, D. (1989). Reaction of atomic hydrogen with crystalline silicon. *Surface science*, 209(3):291–313.

Basile, A. and Nunes, S. P. (2011). *Advanced membrane science and technology for sustainable energy and environmental applications*. Elsevier.

Baticle, P., Kiefer, C., Lakhchaf, N., Larbot, A., Leclerc, O., Persin, M., and Sarrazin, J. (1997). Salt filtration on gamma alumina nanofiltration membranes fired at two different temperatures. *Journal of membrane science*, 135(1):1–8.

Beck, R. E. and Schultz, J. S. (1970). Hindered diffusion in microporous membranes with known pore geometry. *Science*, 170(3964):1302–1305.

Beck, R. E. and Schultz, J. S. (1972). Hindrance of solute diffusion within membranes as measured with microporous membranes of known pore geometry. *Biochimica et Biophysica Acta (BBA)-Biomembranes*, 255(1):273–303.

Benfer, S., Popp, U., Richter, H., Siewert, C., and Tomandl, G. (2001). Development and characterization of ceramic nanofiltration membranes. *Separation and Purification Technology*, 22:231–237.

Bhave, R. (2012). *Inorganic Membranes Synthesis, Characteristics and Applications: Synthesis, characteristics, and applications*. Springer Science & Business Media.

Burggraaf, A. and Cot, L. (2009). Fundamentals of inorganic membrane science and technology, 1996.

Chantong, A. and Massoth, F. E. (1983). Restrictive diffusion in aluminas. *AIChE journal*, 29(5):725–731.

Chen, X., Zhang, W., Lin, Y., Cai, Y., Qiu, M., and Fan, Y. (2015). Preparation of high-flux $\gamma$-alumina nanofiltration membranes by using a modified sol–gel method. *Microporous and Mesoporous Materials*, 214:195–203.

Condom, S., Larbot, A., Younssi, S. A., and Persin, M. (2004). Use of ultra-and nanofiltration ceramic membranes for desalination. *Desalination*, 168:207–213.

Currie, J. (1960). Gaseous diffusion in porous media. part 2.-dry granular materials. *British Journal of Applied Physics*, 11(8):318.

Das, N. and Maiti, H. S. (2009). Ceramic membrane by tape casting and sol–gel coating for microfiltration and ultrafiltration application. *Journal of Physics and Chemistry of Solids*, 70(11):1395–1400.

De Keijser, M. and Van Opdorp, C. (1991). Atomic layer epitaxy of gallium arsenide with the use of atomic hydrogen. *Applied physics letters*, 58(11):1187–1189.

Dendooven, J., Deduytsche, D., Musschoot, J., Vanmeirhaeghe, R., and Detavernier, C. (2009). Modeling the conformality of atomic layer deposition: the effect of sticking probability. *Journal of The Electrochemical Society*, 156(4):P63–P67.

Dendooven, J., Deduytsche, D., Musschoot, J., Vanmeirhaeghe, R., and Detavernier, C. (2010). Conformality of al2o3 and aln deposited by plasma-enhanced atomic layer deposition. *Journal of The Electrochemical Society*, 157(4):G111–G116.

Duscher, S. (2013). Ceramic membranes in chemical and pharmaceutical applications. *Ceramic Applications*, 1(1):19–23.

Elam, J., Routkevitch, D., Mardilovich, P., and George, S. (2003). Conformal coating on ultrahigh-aspect-ratio nanopores of anodic alumina by atomic layer deposition. *Chemistry of Materials*, 15(18):3507–3517.

Ergun, S. (1952). Mass-transfer rate in packed columns-its analogy to pressure loss. *Chemical Engineering Progress*, 48(5):227–236.

Ferguson, J., Yoder, A., Weimer, A., and George, S. (2004). Tio 2 atomic layer deposition on zro 2 particles using alternating exposures of ticl 4 and h 2 o. *Applied Surface Science*, 226(4):393–404.

Fujiwara, H. (2007). *Spectroscopic ellipsometry: principles and applications*. John Wiley & Sons.

Gitis, V. and Rothenberg, G. (2016). *Ceramic membranes: new opportunities and practical applications*. John Wiley & Sons.

Gobina, E. (2006). Apparatus and method for separating gases. US Patent 7,048,778.

Goldsmith, R. L. (1991). Method of forming a porous inorganic membrane on a porous support using a reactive inorganic binder. US Patent 4,983,423.

Goldstein, J., Newbury, D. E., Echlin, P., Joy, D. C., Romig Jr, A. D., Lyman, C. E., Fiori, C., and Lifshin, E. (2012). *Scanning electron microscopy and X-ray microanalysis: a text for biologists, materials scientists, and geologists*. Springer Science & Business Media.

Gordon, R. G., Hausmann, D., Kim, E., and Shepard, J. (2003). A kinetic model for step coverage by atomic layer deposition in narrow holes or trenches. *Chemical Vapor Deposition*, 9(2):73–78.

Greaves, J. and Linnett, J. (1959). Recombination of atoms at surfaces. part 5.—oxygen atoms at oxide surfaces. *Transactions of the Faraday Society*, 55:1346–1354.

Greer, F., Fraser, D., Coburn, J., and Graves, D. B. (2003). Fundamental beam studies of radical enhanced atomic layer deposition of tin. *Journal of Vacuum Science & Technology A: Vacuum, Surfaces, and Films*, 21(1):96–105.

Isobe, T., Kameshima, Y., Nakajima, A., Okada, K., and Hotta, Y. (2006). Extrusion method using nylon 66 fibers for the preparation of porous alumina ceramics with oriented pores. *Journal of the European Ceramic Society*, 26(12):2213–2217.

Kariniemi, M., Niinistö, J., Vehkamäki, M., Kemell, M., Ritala, M., Leskelä, M., and Putkonen, M. (2012). Conformality of remote plasma-enhanced atomic layer deposition processes: An experimental study. *Journal of Vacuum Science & Technology A: Vacuum, Surfaces, and Films*, 30(1):01A115.

Kermanpur, A., Ghassemali, E., and Salemizadeh, S. (2008). Synthesis and characterisation of microporous titania membranes by dip-coating of anodised alumina substrates using sol–gel method. *Journal of Alloys and Compounds*, 461(1):331–335.

Kim, H. and Oh, I.-K. (2014). Review of plasma-enhanced atomic layer deposition: Technical enabler of nanoscale device fabrication. *Japanese Journal of Applied Physics*, 53(3S2):03DA01.

Kim, J.-Y., Ahn, J.-H., Kang, S.-W., and Kim, J.-H. (2007a). Step coverage modeling of thin films in atomic layer deposition. *Journal of applied physics*, 101(7):073502.

Kim, J.-Y., Kim, J.-H., Ahn, J.-H., Park, P.-K., and Kang, S.-W. (2007b). Applicability of step-coverage modeling to tio2 thin films in atomic layer deposition. *Journal of The Electrochemical Society*, 154(12):H1008–H1013.

Kim, W.-H., Park, S.-J., Son, J.-Y., and Kim, H. (2008). Ru nanostructure fabrication using an anodic aluminum oxide nanotemplate and highly conformal ru atomic layer deposition. *Nanotechnology*, 19(4):045302.

Kim, Y. C. and Boudart, M. (1991). Recombination of oxygen, nitrogen, and hydrogen atoms on silica: kinetics and mechanism. *Langmuir*, 7(12):2999–3005.

Knoops, H., Langereis, E., Van De Sanden, M., and Kessels, W. (2010). Conformality of plasma-assisted ald: physical processes and modeling. *Journal of The Electrochemical Society*, 157(12):G241–G249.

Kruczek, B. (2014). Carman–kozeny equation. In *Encyclopedia of Membranes*, pages 1–3. Springer.

Ku, A. Y.-C., Ruud, J. A., Molaison, J. L., Schick, L. A., and Ramaswamy, V. (2008). Functionalized inorganic membranes for gas separation. US Patent 7,396,382.

Kubala, N. G., Rowlette, P. C., and Wolden, C. A. (2009). Plasma-enhanced atomic layer deposition of anatase tio2 using ticl4. *The Journal of Physical Chemistry C*, 113(37):16307–16310.

Kubala, N. G. and Wolden, C. A. (2010). Self-limiting growth of anatase tio 2: A comparison of two deposition techniques. *Thin Solid Films*, 518(23):6733–6737.

Laplante, P. A. (2005). *Comprehensive dictionary of electrical engineering*. CRC Press.

Larbot, A., Alami-Younssi, S., Persin, M., Sarrazin, J., and Cot, L. (1994). Preparation of a $\gamma$-alumina nanofiltration membrane. *Journal of membrane science*, 97:167–173.

Larbot, A., Young, D., Guizard, C., Paterson, R., and Cot, L. (1992). Alumina nanofiltration membrane from sol-gel process. In *Key Engineering Materials*, volume 61, pages 395–398. Trans Tech Publ.

Lee, M., Wu, Z., and Li, K. (2015). 2—advances in ceramic membranes for water treatment. In *Advances in Membrane Technologies for Water Treatment*, pages 43–82. Woodhead Publishing, Oxford.

Li, F., Yang, Y., Fan, Y., Xing, W., and Wang, Y. (2012). Modification of ceramic membranes for pore structure tailoring: The atomic layer deposition route. *Journal of membrane science*, 397:17–23.

Li, K. (2007). *Ceramic membranes for separation and reaction*. John Wiley & Sons.

Lim, J. W., Yun, S. J., and Lee, J. H. (2004). Characteristics of tio2 films prepared by ald with and without plasma. *Electrochemical and solid-state letters*, 7(11):F73–F76.

Lin, C., Flowers, D., and Liu, P. (1994). Characterization of ceramic membranes ii. modified commercial membranes with pore size under 40 å. *Journal of membrane science*, 92(1):45–58.

Lin, Y. and Burggraaf, A. (1993). Experimental studies on pore size change of porous ceramic membranes after modification. *Journal of membrane science*, 79(1):65–82.

Liu, D.-M. (1996). *Porous ceramic materials: fabrication, characterization, applications*. Trans Tech Publ.

Maissel, L. I. and Glang, R. (1970). Handbook of thin film technology. *New York: McGraw-Hill, 1970, edited by Maissel, Leon I.; Glang, Reinhard*.

Majewska-Nowak, K. M. (2010). Application of ceramic membranes for the separation of dye particles. *Desalination*, 254(1-3):185–191.

Marichy, C., Bechelany, M., and Pinna, N. (2012). Atomic layer deposition of nanostructured materials for energy and environmental applications. *Advanced Materials*, 24(8):1017–1032.

Matero, R., Rahtu, A., and Ritala, M. (2001). In situ quadrupole mass spectrometry and quartz crystal microbalance studies on the atomic layer deposition of titanium dioxide from titanium tetrachloride and water. *Chemistry of materials*, 13(12):4506–4511.

McCabe, W. L., Smith, J. C., and Harriott, P. (1993). *Unit operations of chemical engineering*, volume 5. McGraw-Hill New York.

Mitchell, B. S. (2004). *An introduction to materials engineering and science for chemical and materials engineers*. John Wiley Sons.

Mori, H., Mase, S., Yoshimura, N., Hotta, T., Aya-ma, K., and Tsubaki, J. (1998). Mesoporous and microporous titania membranes. *J Membr Sci*, 147:23–33.

Mulder, M. (1991). Basic principles of menbrane technology, klywer academic. *Publishers, London*.

Niskanen, A., Arstila, K., Leskelä, M., and Ritala, M. (2007). Radical enhanced atomic layer deposition of titanium dioxide. *Chemical Vapor Deposition*, 13(4):152–157.

Prechtl, G., Kersch, A., Icking-Konert, G. S., Jacobs, W., Hecht, T., Boubekeur, H., and Schroder, U. (2003). A model for al/sub 2/o/sub 3/ald conformity and deposition rate from oxygen precursor reactivity. In *Electron Devices Meeting, 2003. IEDM'03 Technical Digest. IEEE International*, pages 9–6. IEEE.

Profijt, H., Potts, S., Van de Sanden, M., and Kessels, W. (2011). Plasma-assisted atomic layer deposition: basics, opportunities, and challenges. *Journal of Vacuum Science & Technology A: Vacuum, Surfaces, and Films*, 29(5):050801.

Qi, H., Zhu, G., Li, L., and Xu, N. (2012). Fabrication of a sol–gel derived microporous zirconia membrane for nanofiltration. *Journal of sol-gel science and technology*, 62(2):208–216.

Reichelt, R. (2007). Scanning electron microscopy. In *Science of microscopy*, pages 133–272. Springer.

Ritala, M., Leskela, M., Niinisto, L., and Haussalo, P. (1993a). Titanium isopropoxide as a precursor in atomic layer epitaxy of titanium dioxide thin films. *Chemistry of materials*, 5(8):1174–1181.

Ritala, M., Leskelä, M., Nykänen, E., Soininen, P., and Niinistö, L. (1993b). Growth of titanium dioxide thin films by atomic layer epitaxy. *Thin Solid Films*, 225(1-2):288–295.

Rose, M. and Bartha, J. (2009). Method to determine the sticking coefficient of precursor molecules in atomic layer deposition. *Applied Surface Science*, 255(13):6620–6623.

Rose, M., Bartha, J., and Endler, I. (2010). Temperature dependence of the sticking coefficient in atomic layer deposition. *Applied Surface Science*, 256(12):3778–3782.

Russ, J. C. (2013). *Fundamentals of Energy Dispersive X-Ray Analysis: Butterworths Monographs in Materials*. Butterworth-Heinemann.

Schaep, J., Vandecasteele, C., Peeters, B., Luyten, J., Dotremont, C., and Roels, D. (1999). Characteristics and retention properties of a mesoporous $\gamma$-al 2 o 3 membrane for nanofiltration. *Journal of Membrane Science*, 163(2):229–237.

Schäfer, A. I., Fane, A. G., and Waite, T. D. (2005). *Nanofiltration: principles and applications*. Elsevier.

Seader, J. D., Henley, E. J., and Roper, D. K. (1998). Separation process principles.

Sengupta, A. and Sirkar, K. K. (1995). Analysis and design of membrane permeators for gas separation. *Membrane Science and Technology*, 2:499–552.

Shang, R., Goulas, A., Tang, C. Y., de Frias Serra, X., Rietveld, L. C., and Heijman, S. G. (2017). Atmospheric pressure atomic layer deposition for tight ceramic nanofiltration membranes: Synthesis and application in water purification. *J. Memb. Sci.*, 528(January):163–170.

Shirley, J., Mandale, S., and Kochkodan, V. (2014). Influence of solute concentration and dipole moment on the retention of uncharged molecules with nanofiltration. *Desalination*, 344:116–122.

Skluzacek, J. M., Tejedor, M. I., and Anderson, M. A. (2007). Nacl rejection by an inorganic nanofiltration membrane in relation to its central pore potential. *Journal of membrane science*, 289(1):32–39.

Sondhi, R., Bhave, R., and Jung, G. (2003). Applications and benefits of ceramic membranes. *Membrane Technology*, 2003(11):5–8.

Spillman, R. (1995). Economics of gas separation membrane processes. *Membrane Science and Technology*, 2:589–667.



Strathmann, H. (2001). Membrane separation processes: current relevance and future opportunities. *AIChE Journal*, 47(5):1077–1087.

Strathmann, H., Giorno, L., and Drioli, E. (2011). *Introduction to membrane science and technology*, volume 544. Wiley-VCH Weinheim.

Streitwolf, H. W. (1959). Zur theorie der sekundärelektronenemission von metallen der anregungsprozeß. *Annalen der Physik*, 458(3-4):183–196.

Sutera, S. P. and Skalak, R. (1993). The history of poiseuille's law. *Annual Review of Fluid Mechanics*, 25(1):1–20.

Tiller, F. M. and TSAI, C.-D. (1986). Theory of filtration of ceramics: I, slip casting. *Journal of the American Ceramic Society*, 69(12):882–887.

Tserepi, A. D. and Miller, T. A. (1994). Two-photon absorption laser-induced fluorescence of h atoms: A probe for heterogeneous processes in hydrogen plasmas. *Journal of applied physics*, 75(11):7231–7236.

Uche, D. O. V. (2013). Sol-gel technique: A veritable tool for crystal growth. *Adv. Appl. Sci. Res*, 4:506–510.

Van der Bruggen, B., Schaep, J., Wilms, D., and Vandecasteele, C. (1999). Influence of molecular size, polarity and charge on the retention of organic molecules by nanofiltration. *Journal of Membrane Science*, 156(1):29–41.

Van der Bruggen, B. and Vandecasteele, C. (2002). Modelling of the retention of uncharged molecules with nanofiltration. *Water Research*, 36(5):1360–1368.

Van Gestel, T., Sebold, D., Kruidhof, H., and Bouwmeester, H. J. (2008). Zro 2 and tio 2 membranes for nanofiltration and pervaporation: Part 2. development of zro2 and tio2 toplayers for pervaporation. *Journal of Membrane Science*, 318(1):413–421.

Van Gestel, T., Vandecasteele, C., Buekenhoudt, A., Dotremont, C., Luyten, J., Leysen, R., Van der Bruggen, B., and Maes, G. (2002). Alumina and titania multilayer membranes for nanofiltration: preparation, characterization and chemical stability. *Journal of membrane Science*, 207(1):73–89.

Wenten, I. G. (2002). Recent development in membrane science and its industrial applications. *J Sci Technol Membrane Sci Technol*, 24(Suppl):1010–1024.

Wolf, S. and Tauber, R. N. (1986). Silicon processing for the vlsi era. *Pattern Registration*, pages 473–476.

Wood, B. J. and Wise, H. (1961). Kinetics of hydrogen atom recombination on surfaces1. *The Journal of Physical Chemistry*, 65(11):1976–1983.

Xie, Q., Musschoot, J., Deduytsche, D., Van Meirhaeghe, R. L., Detavernier, C., Van den Berghe, S., Jiang, Y.-L., Ru, G.-P., Li, B.-Z., and Qu, X.-P. (2008). Growth kinetics and crystallization behavior of tio2 films prepared by plasma enhanced atomic layer deposition. *Journal of The Electrochemical Society*, 155(9):H688–H692.

Yacou, C., Wang, D., Motuzas, J., Zhang, X., Smart, S., and Diniz da Costa, J. C. (2013). Thin-film ceramic membranes. *Encyclopedia of Membrane Science and Technology*.